International Journal of Biological Macromolecules 299 (2025) 140208

Contents lists available at ScienceDirect

International Journal of Biological Macromolecules

journal homepage: www.elsevier.com/locate/ijbiomac

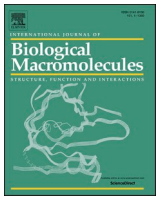

Co-cultivation of *Komagataeibacter sp.* and *Lacticaseibacillus sp.* strains to produce bacterial nanocellulose-hyaluronic acid nanocomposite membranes for skin wound healing applications

M. Brugnoli [a], J.P.F. Carvalho [b], M.P. Arena [a], H. Oliveira [c], C. Vilela [b], C.S.R. Freire [b,*], M. Gullo [a,*]

[a] *Unimore Microbial Culture Collection Laboratory, Department of Life Sciences, University of Modena and Reggio Emilia, 42124 Reggio Emilia, Italy*
[b] *CICECO – Aveiro Institute of Materials, Department of Chemistry, University of Aveiro, 3810-193 Aveiro, Portugal*
[c] *CESAM – Centre for Environmental and Marine Studies, Department of Biology, University of Aveiro, 3810-193 Aveiro, Portugal*

ARTICLE INFO

Keywords:
Bacterial nanocellulose
Co-culture, hyaluronic acid
Komagataeibacter sp.
Lacticaesibacillus casei
Wound healing applications

ABSTRACT

Inspired by natural microbial cooperation, a co-culture approach was used to synthesize bacterial nanocellulose (BNC)-based nanocomposites for potential wound healing applications. By co-culturing either *Komagataeibacter xylinus* (K1G4) or the never tested strain K. rhaeticus (K2G46) with the hyaluronic acid (HA)-producer *Lacticaseibacillus casei* UMCC 2535, two BNC-HA nanocomposites were obtained (C1-K1 and C2-K2). The membranes showed a HA content of 0.49 ± 0.05 mg (C1-K1) and 1.40 ± 0.07 mg (C2-K2), and both revealing a nearly complete release of HA after 1 h in PBS. Compared to pure BNC membranes, the nanocomposites showed enhanced properties, including higher crystallinity (K1G4 = 84.6 %; K2G46 = 76.5 %; C1-K1 = 89.1 %; C2-K2 = 88.1 %), and Young's modulus (K1G4 = 3.38 ± 0.56 GPa; K2G46 = 2.22 ± 0.65 GPa; C1-K1 = 10.00 ± 1.32 GPa; C2-K2 = 7.90 ± 1.54 GPa). Additionally, both BNC-HA membranes exhibited increased moisture uptake (K1G4 = 9.06 ± 0.47 %; K2G46 = 9.27 ± 1.33 %; C1-K1 = 13.65 ± 0.53 %; C2-K2 = 16.26 ± 1.05 %) and water absorption (K1G4 = 82.18 ± 5.25 %; K2G46 = 86.54 ± 7.86 %; C1-K1 = 160.04 ± 9.33 %; C2-K2 = 144.42 ± 13.86 %) capacity. Moreover, they were non-cytotoxic towards human keratinocyte (HaCaT) cells, with >90 % cell viability for up to 72 h. The *in vitro* scratch assays showed a complete wound closure within 48 h for cells exposed to BNC-HA membranes. These findings underscore the potential of co-culturing system to develop BNC-HA nanocomposites for wound healing applications.

1. Introduction

Bacterial nanocellulose (BNC) is a cellulosic substrate produced by various microorganisms, with acetic acid bacteria (AAB) of the *Komagataeibacter* genus, such as *K. xylinus* and *K. rhaeticus*, as the most notable producer strains [1]. BNC is typically cultivated in static conditions, yielding membranes with a high water content. In recent decades, BNC has attracted considerable attention due to its unique set of properties, such as high water-holding capacity, excellent mechanical performance, namely Young's modulus and tensile strength, particularly in the wet state, high purity, and biocompatibility. For example, BNC membranes have been extensively studied as platforms for the fabrication of functional nanocomposite materials [2], thanks to their porous structure and ability to incorporate various natural and synthetic polymers [3–6], drugs [7,8] or even living microorganisms [9,10].

BNC modification strategies can be broadly classified into two main approaches, *viz. ex-situ* and *in-situ*. The *ex-situ* approach involves the incorporation of polymers (or other molecules) after BNC biosynthesis and purification [11], whereas in the *in-situ* approach the integration of the polymers into BNC membranes occurs during the cultivation step [12]. Interestingly, many biopolymers used in these approaches, such as hyaluronic acid (HA), are also naturally secreted by microorganisms. This has led to the development of multi-microbial systems, known as microbial co-culture systems, that allow the incorporation of microbial-based polymers into BNC membranes during microbials co-cultivation. This methodology offers benefits like reduced production costs and fewer pre-treatment steps, and such co-culture systems have been effectively applied to produce BNC-based composites using bacteria,

* Corresponding authors.
E-mail addresses: cfreire@ua.pt (C.S.R. Freire), maria.gullo@unimore.it (M. Gullo).

https://doi.org/10.1016/j.ijbiomac.2025.140208
Received 14 November 2024; Received in revised form 9 January 2025; Accepted 20 January 2025
Available online 21 January 2025

fungi, or consortia inspired by naturally occurring symbiotic systems [13]. These composites combine the desired functional properties with the improved mechanical performance and water-holding capacity of BNC. Depending on the co-culture system and the incorporated (bio) polymer, these functional BNC-based composites show increased potential for fields like biomedicine, particularly as wound dressings [14–17].

In the case of wound healing applications, where various cells engage in complex interactive processes, wound dressings should facilitate and accelerate the healing process. As a natural component of the extracellular matrix of human skin, HA plays a critical role in this process by stimulating epithelial cell responses and activating inflammatory cells, thus enhancing the immune response [18]. For these reasons, HA has been included as a functional additive into BNC matrix through several methods, including *in-situ*, *ex-situ* and, more recently, co-culture approaches [19–21]. However, as far as our literature search could attest, until now, co-culture systems specifically designed for producing BNC-HA nanocomposites predominantly used *K. xylinus* or *Novacetimonas hansenii* strains as BNC producers [21–23], with limited investigation of other species. In fact, there are no previous studies that report *K. rhaeticus* co-cultures with *L. casei* or other lactic acid bacteria, and co-culture systems involving *K. xylinus* and *L. casei* strains are still largely underexplored. Furthermore, although the production of BNC-HA nanocomposite membranes through co-culture systems involving AAB and other bacteria has already been explored [21,22], most of the works focus essentially on the manufacturing procedure, rather than assessing the different strain-dependent and specific properties of the obtained membranes or their potential applications and biocompatibility.

Therefore, the aim of this study was to produce and thoroughly characterize BNC-HA nanocomposites with enhanced properties for potential skin-regeneration applications, such as wound healing, using a co-culture approach involving *K. xylinus* K1G4 (UMCC 2947) or *Komagataeibacter sp.* K2G46 (UMCC 3071), and *L. casei* UMCC 2535. Species-level identification of *Komagataeibacter sp.* K2G46 was conducted prior to co-culturing, as different species can produce BNC membranes with distinct structural characteristics. Two BNC-HA composite membranes were produced: C1-K1 (K1G4-UMCC 2535 combination) and C2-K2 (K2G46-UMCC 2535 combination). In order to clarify the impact of the co-culture procedure on the properties of the nanocomposite membranes and the consequent potential for the desired applications, pure BNC membranes were also prepared for comparison purposes. The BNC yield and HA content (when applicable), morphology, chemical structure, crystallinity, thermal stability, and mechanical properties of the pure BNC and BNC-HA nanocomposites were characterized using scanning electron microscopy (SEM), Fourier-transform infrared spectroscopy with attenuated total reflection (FTIR-ATR), X-ray diffraction (XRD), thermogravimetric analysis (TGA), and tensile tests, respectively. Additionally, water absorption and moisture uptake were evaluated to assess any improvements over pure BNC, and the HA release profiles of the BNC-HA nanocomposites were also evaluated. Finally, *in vitro* cytotoxicity towards human keratinocyte (HaCaT) cells was tested to confirm their safety for skin treatment, and a scratch assay was performed to investigate their effect on cell migration and the potential of the nanocomposite membranes for skin wound healing applications.

2. Materials and methods

2.1. Chemicals, materials and cells

Dimethyl sulfoxide (DMSO, 99.9 %) and 3-(4,5-dimethylthiazol-2-yl)-2,5-diphenyltetrazolium bromide (MTT, 98 %) were obtained from Sigma-Aldrich (Sintra, Portugal). Agarose basic was purchased from AppliChem (Darmstadt, Germany). Dulbecco's Modified Eagle's Medium (DMEM), fetal bovine serum (FBS), phosphate buffer solution (PBS, pH 7.4), L-glutamine, penicillin/streptomycin and fungizone were obtained from Gibco® (Life Technologies, Carlsbad, CA, USA). Other chemicals and solvents were of laboratory grade and used as received. Gluconic acid and lactic acid HPLC standard were purchased from Sigma-Aldrich (Milan, Italy), sulfuric acid 96 % from PanReacAppliChem (ITW Reagents, Milan, Italy), and acetonitrile RS-For HPLC-GOLD-Ultragradient grade from Carlo Erba Reagents (DasitGroup, Milan. Italy).

Bacterial strains K1G4 (UMCC 2947), K2G46 (UMCC 3071), and UMCC 2535 were obtained from UMCC (Unimore Microbial Culture Collection, Reggio Emilia, Italy). The HaCaT cells, a line of non-tumorigenic immortalized human keratinocytes, were obtained from Cell Lines Services (Eppelheim, Germany).

2.2. Culturing conditions and contamination assessment of BNC-producing strains

K1G4, previously identified as *K. xylinus* [24], and K2G46 *Komagataeibacter sp.* strains were initially rehydrated from −80 °C storage conditions and cultivated in Hestrin-Schramm (HS) broth (20.00 g/L glucose anhydrous, 10.00 g/L yeast extract, 5.00 g/L polypeptone, 2.70 g/L disodium phosphate anhydrous, and 1.15 g/L citric acid monohydrate) [25]. UMCC 2535 was cultivated in De Man-Rogosa-Sharpe (MRS) broth (20.00 g/L glucose, 10.00 g/L peptone, 10.00 g/L beef extract, 5.00 g/L yeast extract, 2.00 g/L dipotassium hydrogen phosphate, 5.00 g/L sodium acetate, 2.00 g/L ammonium citrate, 0.20 g/L magnesium sulphate, 0.05 g/L manganous sulphate, and Tween© 80) [26].

A qualitative test on BNC produced after rehydration from −80 °C was conducted following the protocol by Navarro et al. [27] to check for contamination. Pellicles were collected from HS broth, treated with 4 mL of 5 % NaOH, and boiled for 2 h. After the 2-h treatment, if the pellets remained intact, the test was considered positive, indicating no contamination. However, if the pellets dissolved, the samples were considered contaminated. A culture of *K. xylinus* K2G30 (UMCC 2756) was used as a positive control.

2.3. DNA extraction and molecular identification of K2G46 strain

Molecular identification of strain K2G46 was conducted by 16S rRNA gene sequencing. For genomic DNA extraction, K2G46 was cultured in HS medium and incubated aerobically, for 5 days at 28 °C. An aliquot of 8.0 ± 0.1 mL of the cell culture was centrifuged at 10,000*g* (MicroCL 21R, ThermoFisher, US), 4 °C for 10 min. The extraction was performed according to Gullo et al. [28]. After extraction, to check if any contamination occurred, genomic DNA quality was evaluated by gel electrophoresis on 1 % (*w/v*) gel agarose in 1× TBE buffer concentration, while DNA concentration (ng/μL) was measured spectrophotometrically in a NanoDrop™ 1000 Spectrophotometer (Thermo Fisher Scientifc, USA). Band sizes were determined using a 100 bp plus DNA ladder (Invitrogen, Carlsbad, CA, USA). PCR reaction was performed using primers 27F (5'-AGRGTTYGATYMTGGCTCAG-3′) and 1490R (5'-TACGGYTACCTTGTTACGACTT-3′). The amplified product was purified using the kit DNA Clean & Concentrator™-5 (ZymoResearch) and automated sequenced (Sanger sequencing technique, Bio-Fab, Rome, Italy). The Ab1 file was processed using CodonCode aligner 11.0.2 for end-trimming according to primer length, and base quality control. The obtained sequence was aligned against the 16S rRNA database using the blast algorithm (National Center for Biotechnology Information, accessed on 18th May 2024). The K2G46 16S rRNA sequence was deposited in Genbank under the accession number PQ518565.

2.4. Co-culture system

Prior to co-culture assembling, K1G4 and K2G46 were cultivated in HS at 28 °C for 4 days, while UMCC 2535 was cultivated in MRS at 30 °C for 2 days. Two co-culture combinations were formulated, namely: K1G4-UMCC 2535 (C1-K1) and K2G46-UMCC 2535 (C2-K2). Co-

culturing was performed in HS-modified medium according to a previously reported methodology [23]. Strains were co-cultivated in 100 mL Erlenmeyer flasks containing 20.0 ± 0.1 mL with a S/V ratio of 0.8 cm^2/cm^3. Co-cultures were incubated at 30 °C for 3 days in static conditions. UMCC 2535 inoculum was standardized by measuring the optical density of the cultures at 600 nm (OD600) using a UV-6300PC spectrophotometer (VWR, Dallas, TX, USA) and set at a cell's concentration of 10^6 CFU/mL, while AAB inoculum was set at a standard volume (4 % *v/v*).

2.5. Production, harvesting, purification, and quantification of bacterial nanocellulose

For BNC quantification, BNC samples were removed from the spent medium, washed with deionized water 3 times, treated with 0.5 M NaOH at 80 °C for 30 min, and then thoroughly washed with deionized water. BNC-HA samples were collected from the spent media, soaked in 20 mL deionized water, and boiled for 30 min. All samples were then oven-dried at 40 °C until a constant weight was achieved. Dried samples were stored in a desiccator until further use. For quantification, the dried BNC and BNC-HA membranes were weighed using an analytical balance (Pioneer™ Analytical, OHAUS, CH). The weight of the BNC-HA nanocomposites was calculated excluding the HA content. The yield was expressed as grams of BNC produced per liter of culture medium (g/L). Four replicates were analyzed for each sample.

2.6. Analysis of glucose, pH and organic acids

Glucose was determined using enzymatic kit K-SUFRG (Megazyme Ltd. Bray, Ireland). Analyses were performed following the manufacturer's instructions. The concentrations were calculated using MEGACALC. Data and were expressed as grams per liter. pH was measured by using XSPH 80 PRO STIRRER (Securlab, Italy).

Qualitative and quantitative analyses of organic acids was carried out by injecting 20 μL into a Jasco LC-Net II/ADC apparatus equipped with a Jasco pump PU-2080 Plus, and a UV detector set at 210 nm (Jasco UV-2070 Plus). Samples were diluted with distilled water, filtered through 0.45 μm PTFE membranes, and transferred into glass vials for injection. An isocratic separation of molecules was performed using a Bio-Rad Aminex HPX-87H column (300 × 7.8 mm) heated at 40 °C with an Eldex CH-150 oven. The mobile phase was composed of 0.005 N sulfuric acid and 5 % of acetonitrile using a flow of 0.6 mL/min. Peak identifications was conducted using the functions provided by ChromNAV software. Quantitative analysis was performed using standard calibration curves.

2.7. Hyaluronic acid content

BNC-HA samples were removed from spent medium and oven dried at 40 °C. Then, dried BNC-HA samples (diameter: 5 cm) were digested through immersion in distilled water with 1 % *w/v* of cellulase from *Trichoderma viride* (Sigma-Aldrich, Milan, IT). All the samples were incubated for 72 h at 37 °C. The pH of the solution was adjusted at pH 5. After digestion, each sample was centrifuged at 10,000*g* for 10 min at 4 °C, and the supernatants were collected. Then, HA was recovered through precipitation with ethanol, suspended in distilled water, and stored at 4 °C until analysis. The quantification of HA was performed spectrophotometrically following the cetyltrimethylammonium bromide turbidimetric method (CTM) [29] with slight modifications. Briefly, cuvettes were filled with 250.0 ± 0.1 μL of acetate buffer (pH 6) and 250.0 ± 0.1 μL of recovered HA solution. Distilled water was used as control. After incubation at 37 °C for 10 min, 500.0 ± 0.1 μL of the CTM reagent were added to each cuvette, gentle shaken, and incubated at 37 °C for more 10 min. CTM reagent was prepared by dissolving 2.50 ± 0.01 g of cetyltrimethylammonium bromide in a solution of NaOH 2 % *w/v* and heating to 37 °C. Absorbance was read at 400 nm (UV-6300PC, VWR, Dallas, TX, USA). Four replicates were analyzed for each sample.

2.8. Characterization of the BNC-HA membranes

2.8.1. Morphology

Scanning Electron Microscopy (SEM) images of the surface and cross-section of BNC and BNC-HA samples were obtained in a HR-FESEM SU-70 Hitachi microscope (Hitachi High-Technologies Corporation, Tokyo, JP) operating at 4 kV with different magnifications. The samples were placed on a stainless-steel stub and coated with a carbon film before analysis. Cross-section samples were obtained by fracturing in liquid nitrogen.

2.8.2. Fourier-transform infrared–attenuated total reflection spectroscopy (FTIR-ATR)

FTIR-ATR spectra of the BNC and BNC-HA membranes were acquired using a PerkinElmer FT-IR System Spectrum BX (PerkinElmer Inc., Waltham, MA, USA) spectrometer equipped with an ATR single horizontal Golden Gate diamond sensor. The wavenumber range was set from 4000 to 600 cm^{-1} with an accumulation of 32 scans and a resolution of 4 cm^{-1}.

2.8.3. X-ray diffraction (XRD)

XRD was performed using an Empyrean X-ray diffractometer (Malvern Panalytical, Malvern, UK) operating at a voltage of 45 kV and 40 mA using CuKα radiation (λ = 1.541 Å) with a scan rate of 0.05° s^{-1}. Angular range varied from 5 to 40° (2θ). Samples were placed on a Si wafer (negligible background signal) to avoid any bending. Crystallinity index (CI) of each sample was calculated as follows:

$$CI\ (\%) = \left(1 - \frac{I_{am}}{I_{200}}\right) \times 100$$

where, I_{200} is the maximum peak intensity at 2θ around 22° (crystalline region) and I_{am} is the minimum peak intensity at 2θ around 18° (amorphous region).

2.8.4. Thermogravimetric analysis (TGA)

TGA of pure BNC and BNC-HA nanocomposites was carried out with a SETSYS Setaram TGA analyser (SETARAM Instrumentation, Lyon, FR) equipped with a platinum cell. Samples were heated at a constant rate of 10 °C min^{-1}, from room temperature up to 800 °C, under a nitrogen flow of 20 mL/min.

2.9. Mechanical properties

The mechanical performance of dried BNC and BNC-HA membranes was evaluated thorough tensile tests. Analysis was performed in traction mode using a uniaxial Instron 5564 testing machine (Instron Corporation, Norwood, MA, USA) and the crosshead velocity was set at 10 mm min^{-1} using a 500 N static load cell. Samples were cut into rectangular strips (5 × 1 cm^2). The Young's modulus, tensile strength, and the elongation at break were determined using Instron BlueHill 3 software. The thickness of the samples was measured using a hand-held digital micrometre (Mitutoyo Corporation, Tokyo, JP) with an accuracy of 1 μm. All measurements were performed on 5 replicates and the results were expressed as the average value.

2.10. Water absorption

The water absorption capacity was evaluated by placing dried membranes samples at 25 °C for 48 h on an agarose gel (1.4 % *w/v* agarose), as an easy-to-use simulant of physical skin [30]. Samples were weighed at different time points. The percentage of absorbed water was calculated as follows:

$$Water\ absorption\ (\%) = \left(\frac{W_w - W_d}{W_d}\right) \times 100$$

where W_w is the wet weight of the sample at a specific time point, and W_d is the dry weight of the sample.

2.11. Moisture uptake

The moisture uptake capacity of the nanocomposite membranes was assessed by placing dried samples (1×4 cm^2) in a conditioned cabinet with 98 % relative humidity, set using a saturated aqueous solution of potassium sulphate [31], at 25 °C for 48 h. Samples were weighed at different time points and the moisture absorption was calculated as follows:

$$Moisture\ uptake\ (\%) = \left(\frac{W_w - W_d}{W_d}\right) \times 100$$

where W_w is the wet weight of the sample at a specific time point, and W_d is the dry weight of the sample.

2.12. Hyaluronic acid release

HA release from the BNC-HA membranes (diameter: 5 cm) was performed in 30 mL of PBS buffer (pH 7.4) at 37 °C in an orbital shaker set at 120 rpm. At fixed intervals, 5.0 ± 0.1 mL from each sample were collected and substituted with fresh PBS. As reported above, absorbance was read at 400 nm. The cumulative release (%) was calculated as follows:

$$Cumulative\ release\ (\%) = C_n + \left[\frac{(V_r \times C_{n-1})}{V_t}\right]$$

where, C_n and C_{n-1} are the concentrations of HA in solution at times n and n-1; V_r = removed volume; V_t = total volume. Four replicates were analyzed for each sample.

2.13. Cytotoxicity assay

Human keratinocytes cell line (HaCaT cells) was used to evaluate the cytotoxicity of BNC-HA composites and pure BNC through the MTT assay [32]. Cells were cultivated in flasks containing Dulbecco's Modified Eagle's Medium (DMEM) supplemented with 10 % FBS, 2 mM L-glutamine, 10,000 U/mL penicillin/streptomycin and 250 μg/mL fungizone and placed at 37 °C and in a 5 % CO_2 humidified environment. Cultures were examined with an Eclipse TS100 microscope (Nikon, Tokyo, JP) to verify that the cells constituted a subconfluent layer and that their morphology was not altered. Prior to the MTT assay, cells were removed from the flasks through trypsinization. Briefly, cells were first washed with PBS-EDTA, incubated at 37 °C for 10 min, and then treated with a trypsin-EDTA solution and incubated at 37 °C for 5 min. After trypsinization, cells were dispersed in DMEM medium, seeded in 96-wells plates and incubated at 37 °C in a humidified atmosphere containing 5 % CO_2. After 24 h, the medium was removed from each well and substituted with extracts of BNC-HA composites and pure BNC. Extracts were obtained by soaking UV-sterilized 1×1 cm^2 samples in 2 mL of DMEM medium for 24 h. As negative control, cells were exposed to DMEM medium. Cells were exposed to the extracts for 24, 48 and 72 h. At the end of each time point, 50 μL of MTT (1 g/L) were added to each well and incubated at 37 °C, in 5 % CO_2 humidified atmosphere. After 4 h, MTT containing mixture was removed and replaced with 150 μL of DMSO. Plates were placed in an orbital shaker (100 rpm) in the dark for 2 h. The absorbance of the samples was measured at 570 nm with a BioTek Synergy HT plate reader (Synergy HT Multi-Mode, BioTeK, Winooski, VT, USA).

Cell viability (%) was calculated as follows:

$$Cell\ viability\ (\%) = \frac{Abs_{sample}}{Abs_{control}} \times 100$$

where Abs_{sample} is the absorbance of the sample and $Abs_{control}$ is the absorbance of the control.

Two independent assays, with 6 replicates each, were carried out.

2.14. Scratch assay

The effect of the BNC-HA nanocomposite membranes on the migration capability of HaCaT cell lines was evaluated by means of a scratch wound assay [33]. Cells were seeded in 12-wells plates at a concentration of 1×10^5 cells per well. After confluency was reached in each well, a straight scratch was performed using a 200 μL pipette tip. Detached cells were removed by washing twice with PBS buffer. Cells were then exposed for 48 h to BNC-HA and pure BNC extracts, which were prepared as described above. As a negative control, cells were exposed to unaltered DMEM medium. At 24, 30 and 48 h of exposure, optical micrographs of the scratched area of each condition were taken and compared to the negative control.

2.15. Statistical analysis

Experimental data were analyzed and plotted using R v 4.2.3 [34] at a significance level of $p < 0.05$ and reported as average ± standard deviation. Statistical differences were determined by one-way ANOVA and Tukey post-hoc test (between several groups).

3. Results and discussion

The present work focused on the development of BNC-HA nanocomposites membranes, namely C1-K1 and C2-K2, by co-culturing BNC-producers (K1G4 or K2G46) and a HA-producer (UMCC 2535) strains for potential skin wound healing applications (Fig. 1). The used strains were selected based on our previous study [23], in which bacterial strains were screened for their ability to produce BNC and HA, evaluating various strain pairings to assess the feasibility of producing BNC-HA nanocomposites.

Herein, prior to co-culture, the K2G46 strain was identified at species level through 16S rRNA sequencing and analysis. BNC-HA nanocomposite membranes were then produced and characterized regarding their morphology, chemical structure, crystallinity, thermal stability, mechanical properties, water absorption and moisture uptake capacity, and HA release properties. Finally, *in vitro* cytotoxicity and scratch assays with HaCaT cells were carried out to evaluate the biocompatibility and potential wound repair effects of BNC-HA nanocomposite membranes produced through the co-culture approach.

3.1. Identification of acetic acid bacteria species

K1G4 and K2G46 strains were previously isolated from black tea and green Kombucha tea, respectively [35]. K1G4 has undergone whole genome analysis [24], revealing the presence of two fully complete *bcs* operon types and a third copy of *bcsAB*, which correlates with high BNC yields. In addition, by the whole genome analysis, K1G4 has been ascribed to *K. xylinus* species [24]. In the present study, the strain K2G46, deposited as *Komagataeibacter sp.* in the UMCC culture collection, was further identified using 16S rRNA gene sequencing. A BLAST search of its 16S rRNA sequence in GenBank showed over 99.90 % similarity with *K. rhaeticus* strains ENS 9a1, LQ001, and JCM 17122^T. Species characterization is crucial for selecting bacterial strains for BC production since strains from different species can produce BNC membranes with varying morphological characteristics and cellulose I allomorph ratios (I_α/I_β). This variation can be attributed to differences in regulatory networks controlling BNC biosynthesis and species-specific

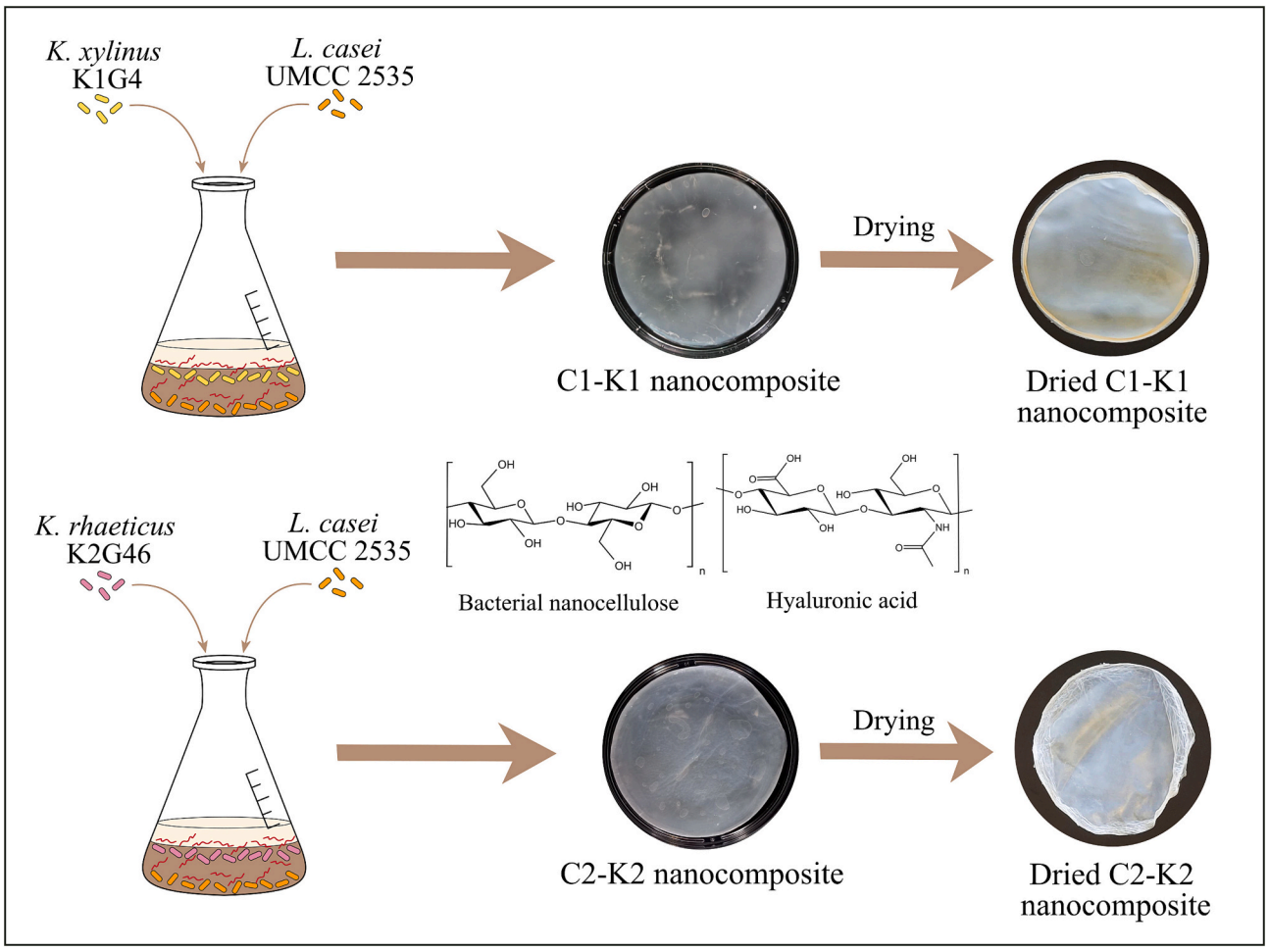

Fig. 1. Schematic representation of the co-culture systems (K1G4-UMCC 2535 and K2G46-UMCC 2535) used to produce BNC-HA nanocomposite membranes (C1-K1 and C2-K2).

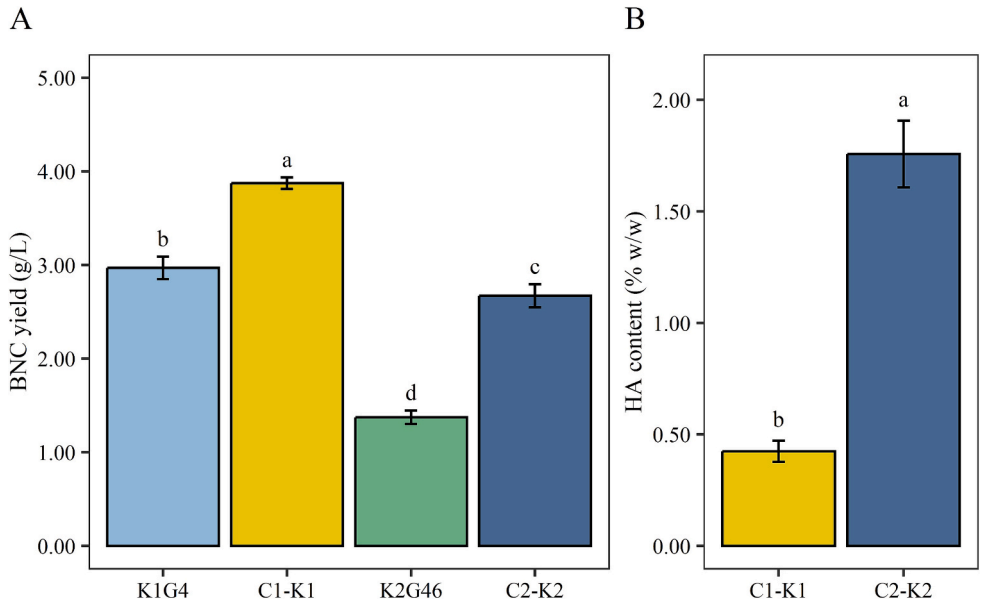

Fig. 2. (A) Quantification of bacterial nanocellulose (BNC) yield (g/L) for pure BNC samples (K1G4 and K2G46) and BNC-HA nanocomposites (C1-K1 and C2-K2). (B) Hyaluronic acid (HA) content (% w/w) in the BNC-HA composites C1-K1, and C2-K2. Data are expressed as mean ± standard deviation (n = 4). Significant differences among values are shown by different letters ($p < 0.05$).

interactions during cellulose microfibril assembly [36,37]. Although *K. rhaeticus* is widely regarded as a model species for BNC production, there are no reports of co-culture systems involving *K. rhaeticus* cultures with *L. casei* or other lactic acid bacteria and aside from this study and our previous work [23], there is no documented evidence of co-culture systems involving *K. xylinus* and *L. casei* strains.

3.2. Effect of the co-culture approach on bacterial cellulose production and hyaluronic acid content

Both K1G4 and K2G46 successfully produced BNC after rehydration, displaying high variability in BNC yield in both monoculture and co-culture. As shown in Fig. 2A, K1G4 yielded 2.97 ± 0.12 g/L of BNC, while K2G46 produced 1.37 ± 0.07 g/L, consistent with the interspecies variability reported in the literature [38]. Compared to K1G4, the lower BNC yield observed in K2G46 can be attributed to its slower glucose consumption (Fig. S1) and higher production of gluconic acid (Fig. S2), which synthesis uses glucose as a carbon source [39]. Significant increases in BNC yield were observed in both C1-K1 and C2-K2 nanocomposite membranes compared to pure BNC produced by K1G4 and K2G46, respectively. The BNC yield increased by 30 % in C1-K1 and by 94 % in C2-K2, with the latter nearly doubling compared to pure BNC from K2G46. C1-K1 achieved the highest yield, reaching 3.87 g/L, indicating that the presence of *L. casei* UMCC 2535 enhanced BNC production for both K1G4 and K2G46 strains. These findings align with similar studies where co-culturing BNC-producing strains with microorganisms belonging to *Bacillus cereus* and *Lactococcus lactis* species increased BNC yield [40,41]. The increased BNC yield is attributable to metabolites produced by *L. casei* UMCC 2535, particularly lactic acid, that can stimulate cell growth and enhance the tricarboxylic acid (TCA) cycle, providing additional energy during the early growth stages. In both co-culture systems, UMCC 2535 successfully produced lactic acid which was metabolized by both K1G4 and K2G46, as confirmed by the decrease in lactic acid concentration at 72 h (Fig. S3). This metabolic boost likely accelerates BNC synthesis by the BNC-producing strains, leading to a higher overall yield [42].

As shown in Fig. 2B, C2-K2 was composed of 1.76 % *w*/w of HA, a content four times higher than th that of C1-K1 (0.43 % *w*/w). This difference could be attributed to the higher BNC production by K1G4, which may limit glucose availability for HA production. Although BNC and HA production involve distinct metabolic pathways, both utilize glucose as a primary carbon source. In HA synthesis, glucose is phosphorylated by hexokinase to produce glucose-6-phosphate (G6P), which is then converted through two distinct pathways into glucuronic acid and *N*-acetylglucosamine, the main HA building blocks [43]. Similarly, when glucose is used as the main carbon source, BNC synthesis begins with glucose phosphorylation to G6P, followed by its conversion to glucose-1-phosphate and UDP-glucose, which is the main BNC precursor [44]. Therefore, as glucose is the initial carbon source in the synthesis of both HA and BNC, an increased BNC production may reduce glucose availability for HA synthesis. In addition, variations in glucose assimilation rates among different *Komagataeibacter* strains, with K1G4 producing BNC and consuming glucose faster than K2G46, may also contribute to this difference [36,37]. In lactic acid bacteria, carbon source utilization for metabolites production is mainly focused on lactic acid production, limiting the carbon source availability for HA production. Additionally, HA synthesis requires more complex enzymatic steps than BNC production [45].

Since the pH of the medium, specifically below 4 and above 11 [46], can affect HA properties and, therefore, its inclusion into the BNC matrix, the pH fluctuations were recorded across the incubation period.

Tthe pH fluctuations (Fig. S4) remained within the stability range, ensuring the integrity of HA during production and incorporation into the nanocomposites. Furthermore, it was observed that the pH differences between C1-K1 (4.41 ± 0.03 after 72 h) and C2-K2 (4.39 ± 0.03 after 72 h) systems were negligible and unlikely to have a significant impact on HA properties. Finally, the higher BNC content, along with the nanofiber structure and crystallinity, could act as a physical barrier, limiting HA integration into the BNC network.

3.3. Nanocomposites' morphology and structural characterization

The effects of the co-culture approach on BNC morphology were evaluated using SEM. As shown in Fig. 3, all samples exhibited a randomly oriented 3D nanofiber network, with both BNC-HA nanocomposite membranes (Fig. 3B and D) showing a denser morphology compared to those of the pure BNC samples (Fig. 3A and C). The cross-sectional micrographs also displayed the typical lamellar microstructure characteristic of BNC [47]. The nanofiber's width was determined by analysing 100 randomly chosen ribbons for each sample, with BNC-HA composites showing nanofibers with larger diameters. Specifically, the average fiber diameters (Fig. 3E) increased from 60 nm for both K1G4 and K2G46 to 84 nm and 95 nm for C1-K1 and C2-K2, respectively. These findings align with a previous study by Liu & Catchmark [22], which reported a significant increase in BNC nanofiber's width when co-cultivating *Novacetimonas hansenii* (formerly known as *Gluconacetobacter hansenii*) ATCC 23769 with the HA producer *Lactococcus lactics* APJ3 in a two-vessel circulating system, which may be explained based on the fact that HA may promote the bundling of cellulose microfibrils, leading to the formation of larger cellulose ribbons [48].

The incorporation of HA into the BNC membranes during co-cultivation was confirmed by FTIR analysis. The spectra (Fig. 4A) of the pure BNC samples displayed characteristic peaks of cellulosic substrates, with the main bands at 3342 cm^{-1} (O—H stretching vibration), 2886 cm^{-1} (C—H stretching vibration), 1427 cm^{-1} (CH_2 bending vibration), 1315 cm^{-1} (O—H bending vibration), and 1031 cm^{-1} (C—O stretching vibration) [30,49], confirming the purity of BNC membranes produced using these strains. In contrast, the BNC-HA nanocomposites showed, in addition to the typical cellulose peaks, strong vibrations around 1640 cm^{-1} (N—H bending amide II and COO^- asymmetric stretching) [30,48] and 1560 cm^{-1} (secondary amide N—H bending and C—N stretching) [48,50] confirming the successful incorporation of HA during co-cultivation. The higher intensity of these peaks in the spectrum of C2-K2 further confirmed its higher HA content.

The diffraction patterns of the BNC and BNC-HA composites revealed the characteristic reflections of cellulose I (Fig. 4B). The first peak at around 15° corresponds to the (100) plane of I_α or the (110) plane of I_β cellulose allomorphs, the second peak at around 17° corresponds to the (010) plane of I_α or (110) plane of I_β, and the peak at around 23° corresponds to the (110) plane of I_α and the (200) plane of cellulose I_β [51,52]. The most intense peaks in the diffractograms of K1G4 and C1-K1 appeared at 2θ around 23°, while in K2G46 and C2-K2, the diffraction at 2θ around 15° had comparable intensity to the 23° peak. As Tang et al. [20] reported, the high intensity of the 15° peak may indicate a predominance of the cellulose I_α allomorph (one-chain triclinic crystal structure). Similar results have been reported in previous studies after testing BNC production by different bacterial species, revealing variations in the cellulose I allomorph ratio (I_α/I_β) between membranes [53,54]. These differences could be attributed to several factors: (i) species-specific regulatory netwoks controlling cellulose biosynthesis, (ii) varying assembly processes of cellulose microfibrils into crystalline structures depending on species-specific interactions, or (iii) differential expression of cellulose synthase genes affecting allomorph composition [54–56].

After co-cultivation, both BNC-HA nanocomposites exhibited higher crystallinity than the pure BNC samples, highlighting the significant influence of the co-culture approach on BNC crystallinity. Specifically, the crystallinity was 84.6 % for K1G4, 89.1 % for C1-K1, 76.5 % for K2G46, and 88.1 % for C2-K2. These results are consistent with the findings of Jiang et al. [57], who reported increased BNC crystallinity when co-cultivating *K. nataicola* with *Limosilactobacillus fermentum* (formerly known as *Lactobacillus fermentum)*. The authors suggested that

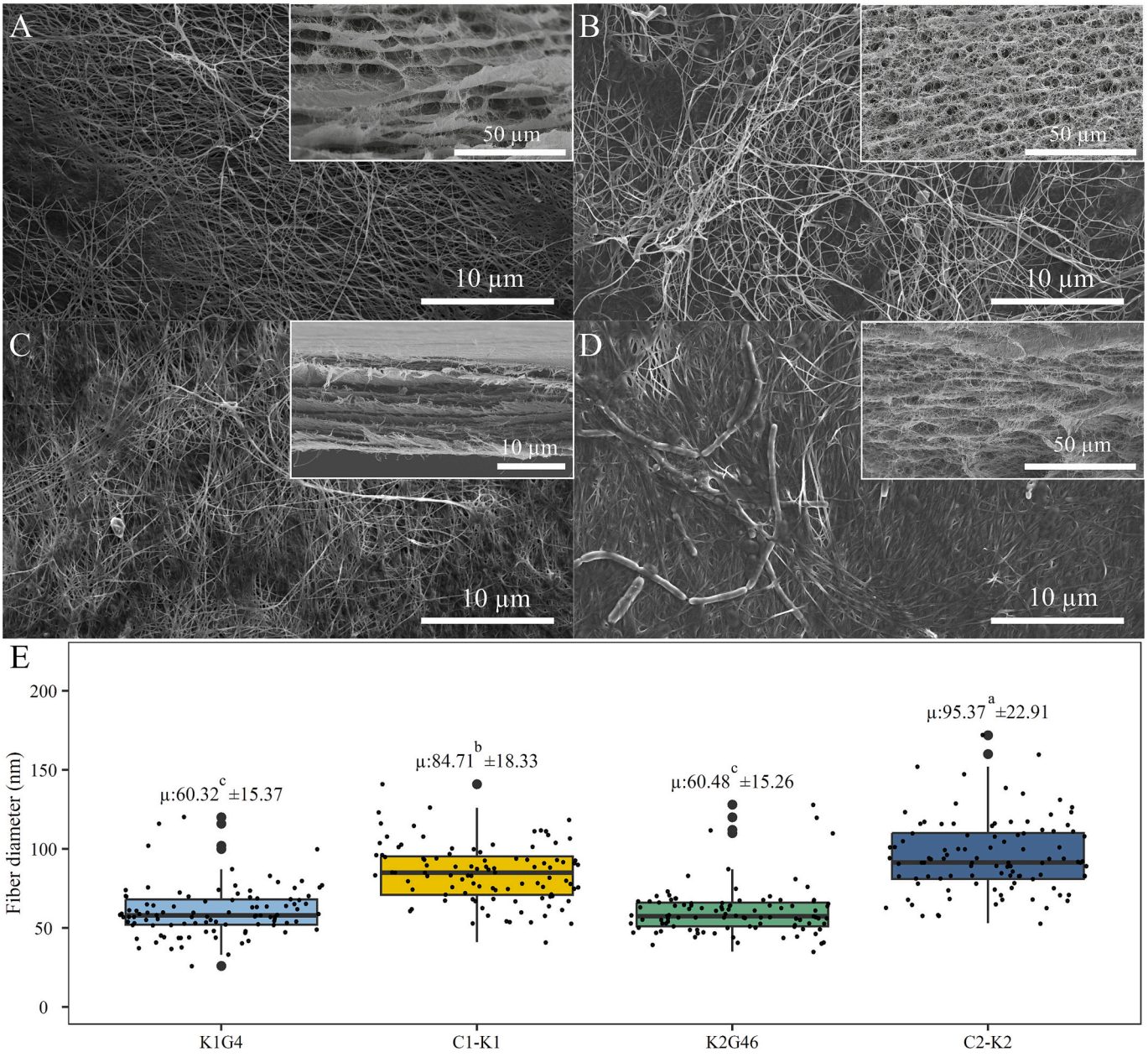

Fig. 3. Scanning electron microscopy images of the surface and cross-section (inserts) of (A) K1G4, (B) C1-K1, (C) K2G46, and (D) C2-K2 samples. (E) The boxplots show the fiber diameter distribution in each sample. "µ" indicates the average diameter (nm) ± standard deviation of 100 randomly chosen nanofibers of bacterial cellulose. Significant differences among fiber diameter are shown by different letters ($p < 0.05$).

synergistic interactions during co-culture could enhance BNC synthesis. Hence, *L. casei* UMCC 2535 possibly provided precursors or cofactors like lactic acid, which are beneficial for cellulose synthesis. This combined metabolic activity could enhance both BNC production and crystallinity. Moreover, Chi & Catchmark [58] observed that exopolysaccharides could modulate microfibril bundling, thereby influencing crystallization. In this study, HA may have influenced cellulose chain arrangement, promoting ordered cellulose assembly.

The thermal stability and degradation profiles of the nanocomposites were evaluated using thermogravimetric analysis. The thermograms of the BNC-HA nanocomposite membranes are very similar to that of pure BNC with a single weight-loss profile (Fig. 4C) [59]. This behaviour can be attributed to the fact that HA is a minor component in the nanocomposites sample weight, as previously described. A similar phenomenon was observed by de Oliveira et al. [19], who reported that BNC-HA membranes, produced *via* an *in-situ* approach, also exhibited a single weight-loss profile, further supporting this observation.

For all samples, the major mass loss occurred between 250 °C and 450 °C (Fig. 4C). The maximum degradation temperatures for pure BNC were recorded at 346.9 °C for K1G4, and 360.6 °C for K2G46, while for BNC-HA composites, these temperatures were of 348.6 °C for C1-K1, and 359.3 °C for C2-K2. These results are comparable to that of BNC-HA membranes produced through *ex-situ* methods, with maximum degradation temperatures reported in the range of 350–360 °C. [19]. Interestingly, membranes with similar crystalline structures and cellulose I_β allomorph compositions (*e.g.*, K1G4 and C1-K1) displayed similar maximum decomposition temperatures. BNC's thermal stability is known to be influenced by its crystallinity, with higher crystallinity generally resulting in improved thermal stability [60]. In this study, pure BNC membranes exhibited lower mass loss up to 200 °C (K1G4 = 6.0 % and K2G46 = 5.7 %) compared to the corresponding BNC-HA nanocomposites (C1-K1 = 5.2 % and C2-K2 = 4.9 %), suggesting

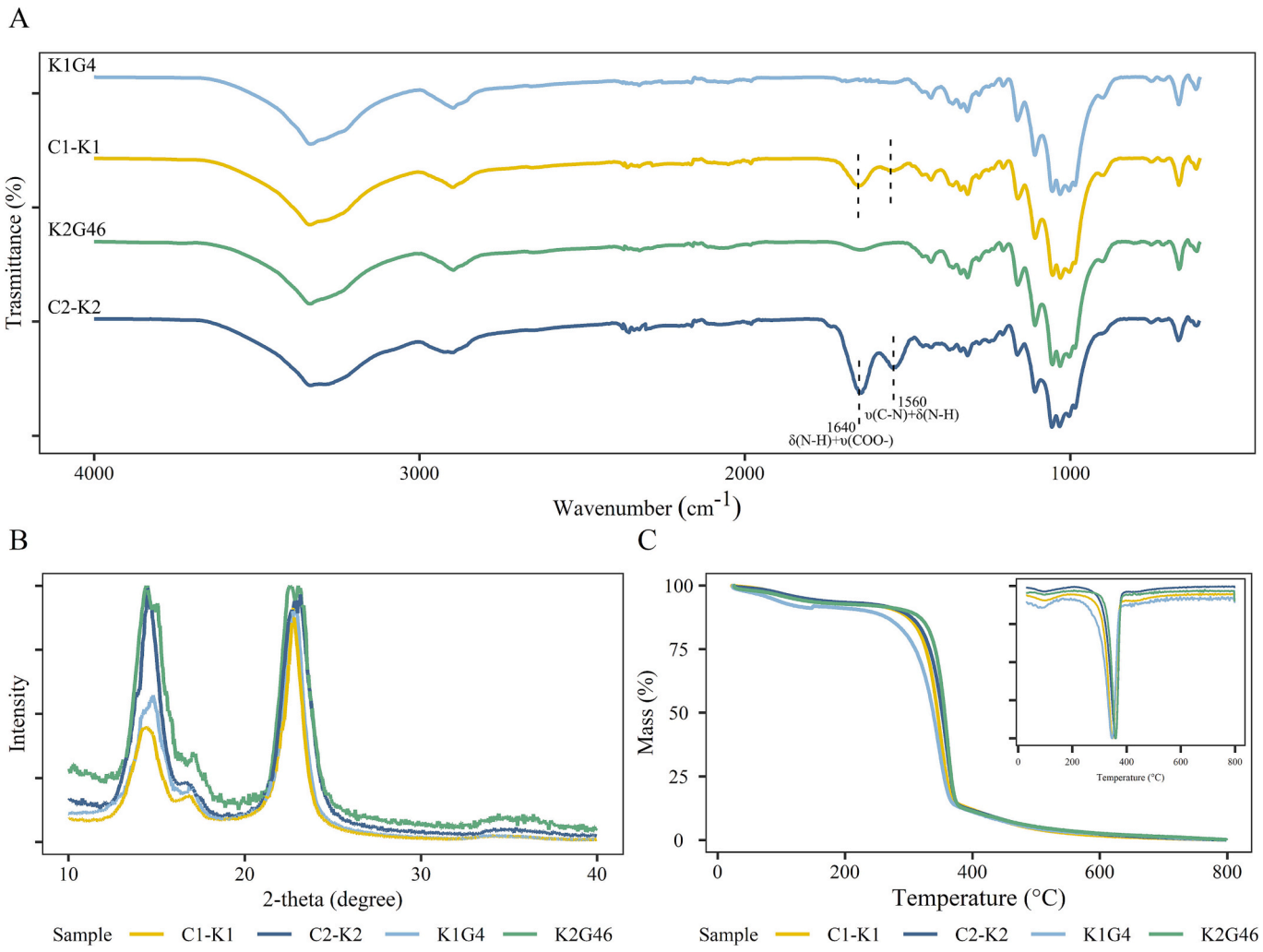

Fig. 4. (A) FTIR spectra of the pure BNC samples (K1G4 and K2G46) and BNC-HA nanocomposites (C1-K1 and C2-K2). (B) XRD patterns of the pure BNC samples and BNC-HA nanocomposites. (C) Thermogravimetric curves and the respective derivatives (insert) of pure BNC and BNC-HA composites.

enhanced thermal stability in the composites, likely due to the strong interaction between HA and BNC molecules [61]. Additionally, the minor weight loss from room temperature to 100 °C can be attributed to the volatilization of residual water. Overall, the thermal stability of both C1-K1 and C2-K2 up to 200 °C suggests they can withstand the sterilization processes (around 150 °C) required for most biomedical applications.

3.4. Mechanical properties

The mechanical performance of the BNC-HA nanocomposite and pure BNC membranes was evaluated through tensile tests. The thickness of the membranes was 0.019 ± 0.030 mm, 0.032 ± 0.001 mm, 0.017 ± 0.03 mm, and 0.032 ± 0.030 mm for K1G4, C1-K1, K2G46, and C2-K2 membranes, respectively. As depicted in Fig. 5A, no differences in terms of elongation at break were observed between either the BNC-HA nanocomposites or pure BNC. On the other hand, the co-culture approach significantly enhanced both Young's modulus (Fig. 5B) and tensile stress at break (Fig. 5C) of the nanocomposites in comparison with pure BNC. However, no substantial differences in Young's modulus (Fig. 5B) were observed between K1G4 (3.38 ± 0.57 GPa) and K2G46 (2.22 ± 0.65 GPa) samples. Nonetheless, a notable 3-fold increase was recorded for C1-K1 K1 (10.00 ± 1.32 GPa) compared to K1G4 and nearly a 4-fold increase for C2-K2 (7.90 ± 1.54 GPa) in respect to K2G46. In terms of tensile stress at break (Fig. 5C), K1G4 exhibited a higher value (53.3 ± 18.4 MPa) than K2G46 (10.64 ± 2.65 MPa). Similar to Young's modulus, the co-culture approach significantly boosted tensile strength, with C1-K1 (156.00 ± 17.4 MPa) showing a 3-fold increase compared to K1G4, and C2-K2 (154.53 ± 12.56 MPa) exhibiting an almost 15-fold increase in comparison to K2G46. These enhancements in Young's modulus and tensile stress at break highlight the positive impact of the co-culture approach on the mechanical properties, likely due to increased BNC content and crystallinity.

The results obtained in the present study are contradictory to those reported in a previous study [21], where co-culturing a *N. hansenii* strain with an engineered *L. lactis* strain resulted in a reduction of Young's modulus and no effect on tensile stress at break in BNC-HA nanocomposites. These results highlight the impact of the specific bacterial strains used in co-culture on enhancing the mechanical properties of BNC-HA composites, underscoring the critical role of bacterial strains selection in designing and optimizing co-culture systems for producing BNC-HA nanocomposites. Additionally, BNC-HA nanocomposites produced through co-culture offer several advantages over those produced *via* conventional *in-situ* or *ex-situ* approaches that generally exhibit diminished mechanical properties compared to pure BNC [20,62].

For applications such as wound dressing or skin repair, specific tensile characteristics are essential for a good adaptation to irregular skin surfaces. According to literature, the Young's modulus of human epidermal skin ranges from approximately 2.9 to 150 MPa, depending on the donor and skin site [63–65]. Both BNC-HA nanocomposite

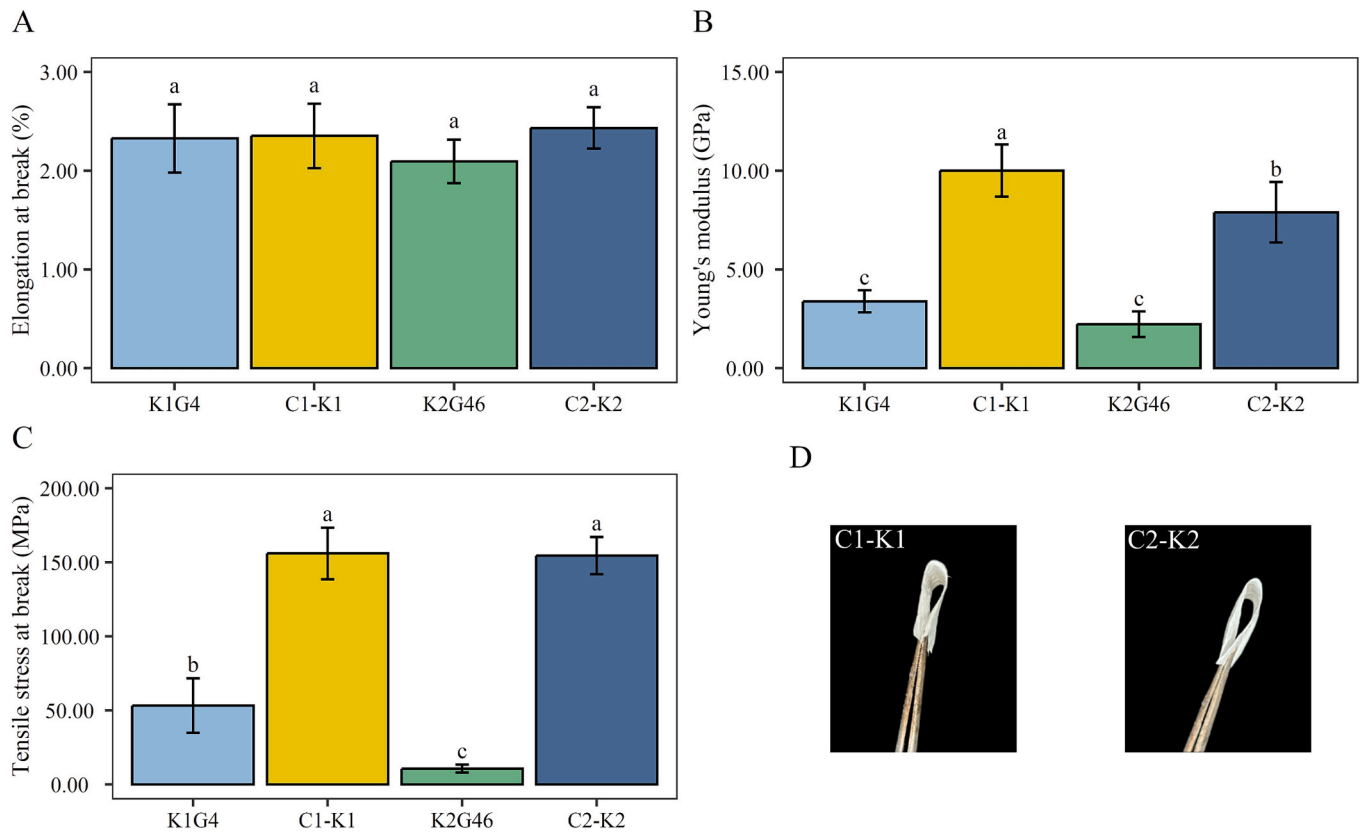

Fig. 5. Tensile tests results: (A) elongation at break, (B) Young's modulus, and (C) tensile stress at break of the pure BNC samples (K1G4 and K2G46) and BNC-HA nanocomposites (C1-K1 and C2-K2). Bar plots indicate the average values of five replicates ± standard deviation. Significant differences among values are shown by different letters ($p < 0.05$). (D) Digital photographs of bent BNC-HA nanocomposites.

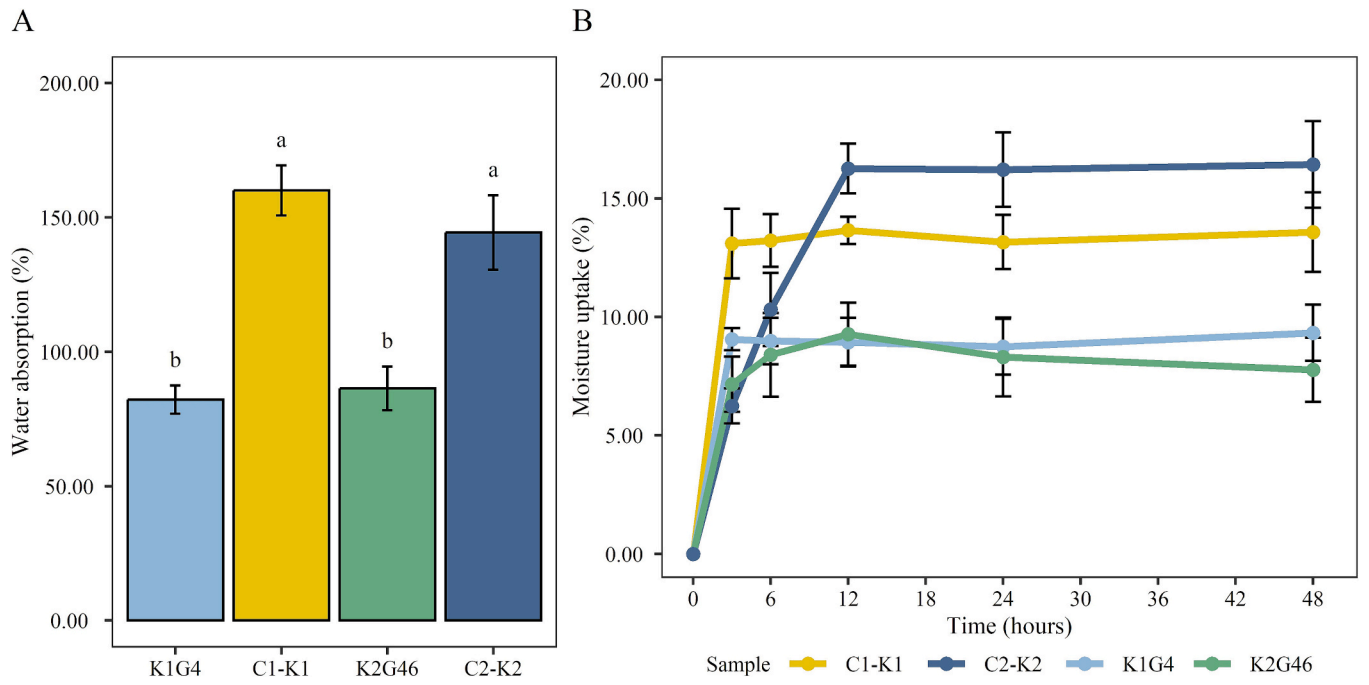

Fig. 6. (A) Water absorption capacity of pure BNC samples (K1G4 and K2G46) and BNC-HA composites (C1-K1 and C2-K2) after 48h; (B) water-uptake of pure BNC samples (K1G4 and K2G46) and BNC-HA composites (C1-K1 and C2-K2) during 48 h. Bar plots indicate the average values by five replicates ± standard deviation. Significant differences among values are shown by different letters ($p < 0.05$).

membranes developed in this study exhibited higher Young's modulus values compared to human epidermal skin, indicating increased stiffness. However, despite the enhanced stiffness, as shown in Fig. 5D, both the C1-K1 and C2-K2 nanocomposites present good pliability. This combination of stiffness and flexibility might be beneficial for wound healing applications, where the BNC-HA nanocomposites can serve as absorbent membranes, provide a barrier function, and facilitate controlled drug release, thereby improving the effectiveness of topical treatments.

3.5. Water absorption and moisture uptake

Water absorption and moisture uptake are crucial indicators of BNC's rehydration ability, significantly impacting exudate absorption when adhered to damaged skin surfaces [66]. Herein, water absorption capacity was assessed by placing the membranes on an agarose hydrogel (1.4 wt%). The samples were gently pressed to ensure full contact with the hydrogel surface. No significant differences were found on the water absorption capacity between K1G4 (82.18 ± 5.25 %) and K2G46 (86.54 ± 7.86 %), the pure BNC membranes (Fig. 6A). However, the BNC-HA nanocomposite membranes exhibited significantly higher values (C1-K1 = 160.04 ± 9.33 %; C2-K2 = 144.42 ± 13.86 %), far exceeding those of the pure membranes. Despite C2-K2 having a higher HA content, no significant difference in water uptake was observed between C1-K1 and C2-K2, probably due to C1-K1's denser structure with smaller pores. Membranes with larger porous structures can trap more water molecules, leading to increased water absorption [67]. Moreover, the BNC-HA nanocomposite membranes adhered well to the agarose hydrogel and maintained their integrity after removal, suggesting that they could effectively adhere to human skin and absorb exudates.

Regarding moisture uptake, the obtained results revealed distinct absorption profiles (Fig. 6B). K1G4 rapidly absorbed moisture, reaching an equilibrium plateau (9.06 ± 0.47 %) within 3 h, while K2G46 took 12 h to reach the equilibrium (9.27 ± 1.33 %). Similarly, C1-K1 quickly reached an equilibrium plateau (13.65 ± 0.53 %) within 3 h, and C2-K2 showed a more gradual absorption profile, reaching 6.24 ± 0.74 % of absorption after 3 h and 10.31 ± 1.54 % after 6 h, before stabilizing at 16.26 ± 1.05 % after 12 h. Both C1-K1 and C2-K2 absorbed more moisture than the pure BNC membranes, with C2-K2 demonstrating the highest absorption capacity. The moisture uptake was certainly influenced by the HA content and the density and arrangement of nanofibers within the membrane. A higher HA content enhances moisture uptake because of the hygroscopic nature of this biopolymer, while a denser fiber structure may reduce it [67]. Consequently, the lower HA content and denser structure of C1-K1 could explain its lower moisture absorption compared to that of C2-K2. These results are in line with previous studies that reported improved water and moisture uptake for BNC-HA membranes obtained by *ex-situ* methodology [30].

3.6. Hyaluronic acid release

The cumulative release of HA from the C1-K1 and C2-K2 nanocomposite membranes was monitored over a 4-h period in PBS, as shown in Fig. 7. The release profiles revealed significant differences between the two samples. C2-K2 displayed an initial burst release of 72 % within the first 10 min, reaching 93 % within 1 h, indicating an immediate release behaviour. This rapid release can be attributed to HA's hydrophilic nature, which facilitates quick diffusion of the buffer into the BNC-HA composite, promoting its release [68]. In contrast, C1-K1 demonstrated a more gradual release, with only 30 % of HA released in the first 10 min and 84 % within 1 h, reflecting a more sustained release profile. These differences are, once more, likely influenced by the HA content and the structural characteristics of the BNC-HA nanocomposite membranes. As already shown in Fig. 2B, C2-K2 contained the highest HA content (1.76 ± 0.15 % *w*/w) compared to C1-K1 (0.43 ± 0.05 % w/w). Close monitoring of the pH during the release study revealed that they were comparable for the C1-K1 and C2-K2 systems, staying between 7.2 and 7.4 in PBS. Since HA is stable under this pH range [46], the structural features and HA content of the nanocomposite membranes, rather than pH fluctuations, are responsible for the observed variations in release patterns. This emphasizes even more how membrane composition and morphology affect HA release kinetics, as the data makes clear. Additionally, the composite membrane morphology plays a crucial role in the HA-release profiles, with higher crystallinity being generally associated with slower drug release kinetics [68]. Furthermore, composites with denser, more organized structures and smaller pore sizes also tend to hinder drug dissolution and release [69]. This is consistent with the obtained data, as C1-K1, which exhibited the slowest release profile, had the lowest HA content (depicted in Fig. 2) and a structure characterized by more regular and

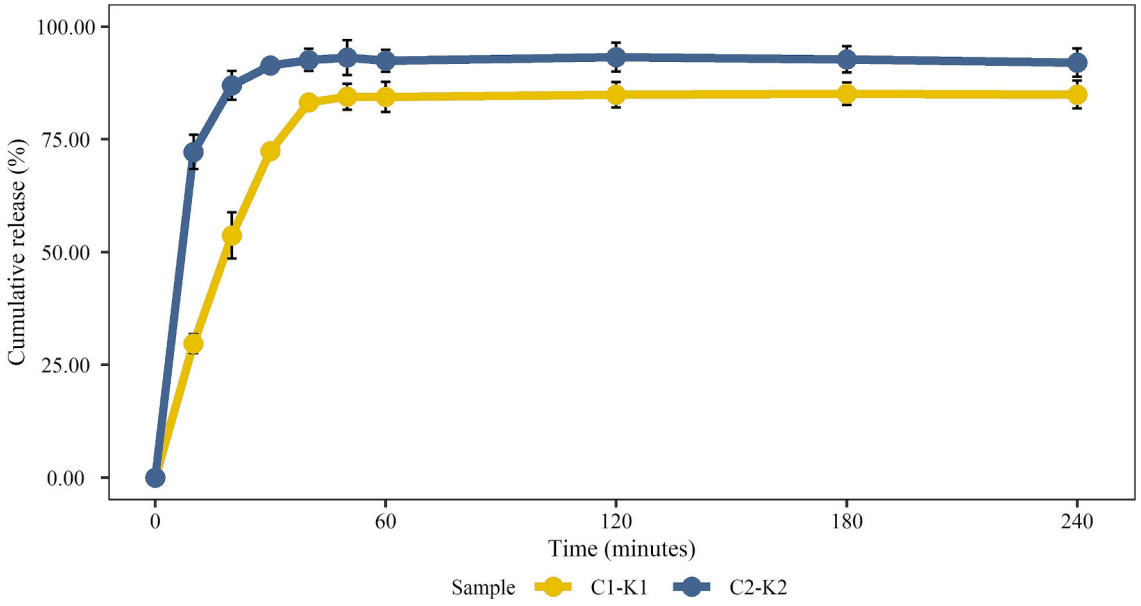

Fig. 7. Cumulative release (%) profile of HA from membranes C1-K1 and C2-K2. Aliquots were collected after 10, 20, 30, 40, 50, 60, 120, 180 and 240 min. Data are expressed as mean ± standard deviation (n = 4).

smaller pores (seen in Fig. 3). Therefore, both the HA content and the nanocomposite morphology significantly affect the HA release kinetics in these BNC-HA nanocomposites. However, the fast release of both nanocomposites aligns with the needs of acute wound management, which requires a prompt therapeutic action to stimulate the healing process [70]. Additionally, these BNC-HA nanocomposites will serve as a physical barrier complementing the effect of HA.

3.7. *In vitro cytotoxicity evaluation*

The cytotoxicity of the BNC-HA nanocomposites was evaluated by exposing HaCaT keratinocyte cells to extracts of the nanocomposites for up to 72 h in order to assess their safety for skin applications, and the obtained cell viability outcomes are shown in Fig. 8. In this case, no significant differences were observed between the control (100 % cells viability) and the BNC and BNC-HA nanocomposites, after 24, 48 and 72 h. The cell viabilities of C1-K1 and C2-K2 extracts ranged from 90.81 to 108.33 % and 91.67 to 110.09 % respectively, which are safely above the 70 % threshold defined by ISO 10993-5:2009 [71]. These results agree with the nature of the components of the developed membranes: previous studies have proven that pure BNC has no cytotoxic effects on various cells lines [72] and HA is employed in several biomedical and pharmaceutical formulations (*e.g.,* cosmetic products) and its non-cytotoxicity to HaCaT cells line has already reported [73]. Moreover, these outcomes are also consistent with the non-cytotoxicity of *ex-situ* and *in-situ* synthetized BNC-HA composites on various cells lines [20,30,74]. Hence, these results indicate the biocompatibility of BNC-HA nanocomposites towards HaCaT cells, confirming the suitability and the safety of the co-culture approach to produce functionalized BNC for skin-related applications.

3.8. *In vitro evaluation of wound healing ability*

An *in vitro* scratch assay was carried out to investigate the wound healing ability of HaCaT cells when exposed BC-HA nanocomposites' extracts. After the creation of a scratch, the wound healing process was followed by optical observations until wound closure. Interestingly, the extent of wound healing was keenly dependent on the presence and content of HA. As can be observed in the micrographs (Fig. 9), cells exposed to BNC-HA extracts showed a faster closure at 24 h and a complete wound closure at 48 h. On the other hand, open wounds were still present in the control and in the samples exposed to pure BNC. This difference was mainly related to the capacity of HA to promote cell migration and wound closure [75]. Similar results have been described by Silva et al. [76], for layered bacterial nanocellulose patches loaded with acyclovir and HA.

4. Conclusions

This work aimed to produce BNC-HA nanocomposite membranes using a co-culture approach combining either *K. xylinus* K1G4 or *K. rhaeticus* K2G46 with *L. casei* UMCC 2535 and thoroughly comparing the properties of the nanocomposite membranes with pure BNC counterparts, in order to obtain materials with improved characteristics for wound-healing applications. In fact, the exploitation of the co-culture approach with BNC and HA producing bacteria successfully generated BNC-HA nanocomposite membranes with adequate properties for application in skin regeneration. Both nanocomposites showed increased BNC yield, namely 3.87 ± 0.06 (C1-K1) and 2.67 ± 0.12 (C2-K2) g/L, and a HA content of 4.25 ± 0.48 (C1-K1) and 17.57 ± 1.50 mg/g dried BNC (C2-K2). Generally, both BNC-HA nanocomposites showed thermal stability up to 200 °C, good mechanical performances (Young's modulus >6.5 GPa and tensile stress at break >138 MPa), and high moisture (C1-K1 = 13.65 ± 0.53 %; C2-K2 = 16.26 ± 1.05 %) and water (C1-K1 = 160.04 ± 9.33 %; C2-K2 = 144.42 ± 13.86 %) uptake capacity. HA release was observed to be 84 % in C1-K1 and 93 % in C2-K2 after 1 h. Finally, the *in vitro* cytotoxicity and the *in vitro* migration assays showed the non-cytotoxicity of both BNC-HA composites towards HaCaT cells, and highlighted the stimulating effect towards cells migration, suggesting that the membranes can promote the wound occlusion due to HA presence. Hence, BNC-HA composites obtained through a co-culture approach may have several advantages over *ex-situ*

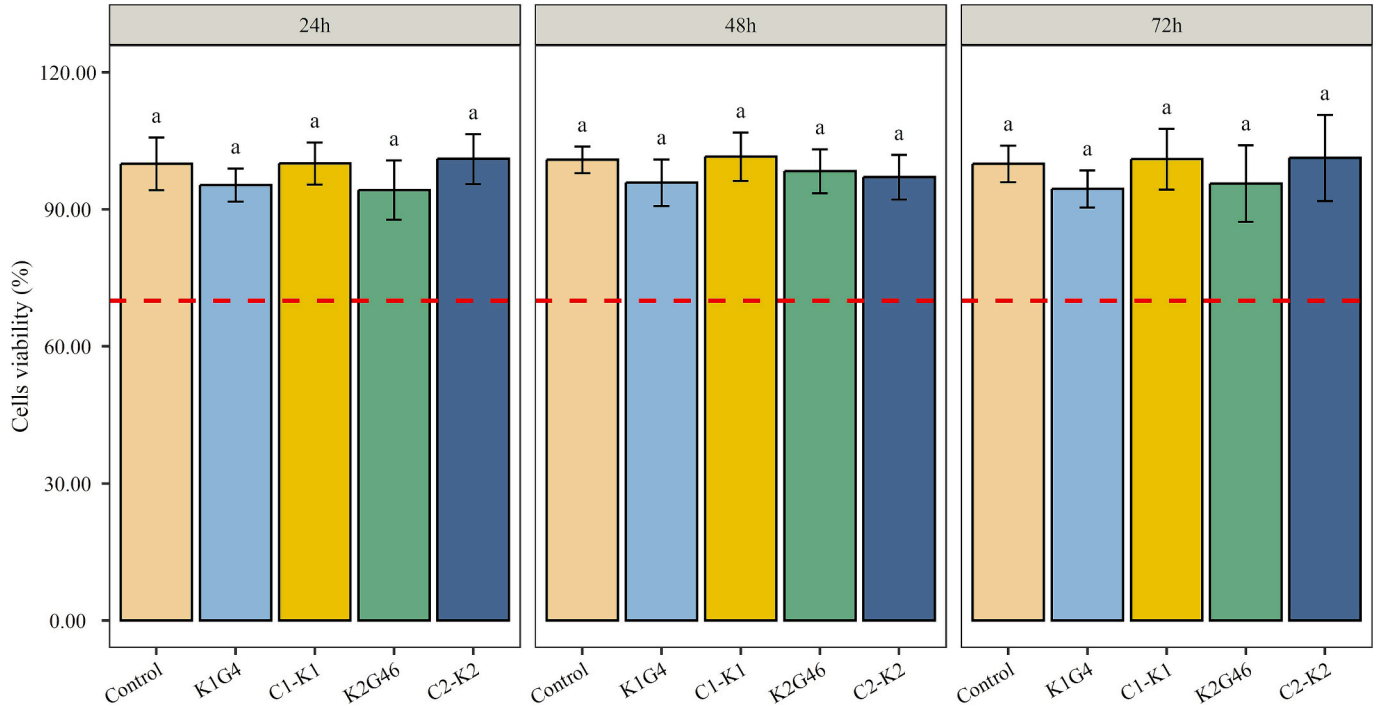

Fig. 8. HaCaT cell viability after exposure to pure BNC (K1G4 and K2G46) and BNC-HA composites (C1-K1 and C2-K2) for 24 h, 48 h, and 72 h. The red dotted line represents the 70% threshold of cells viability defined by ISO 10993-5:2009 [65]. Bar plots indicate the average values by five replicates ± standard deviation. Significant differences among cells viability values are shown by different letters ($p < 0.05$).

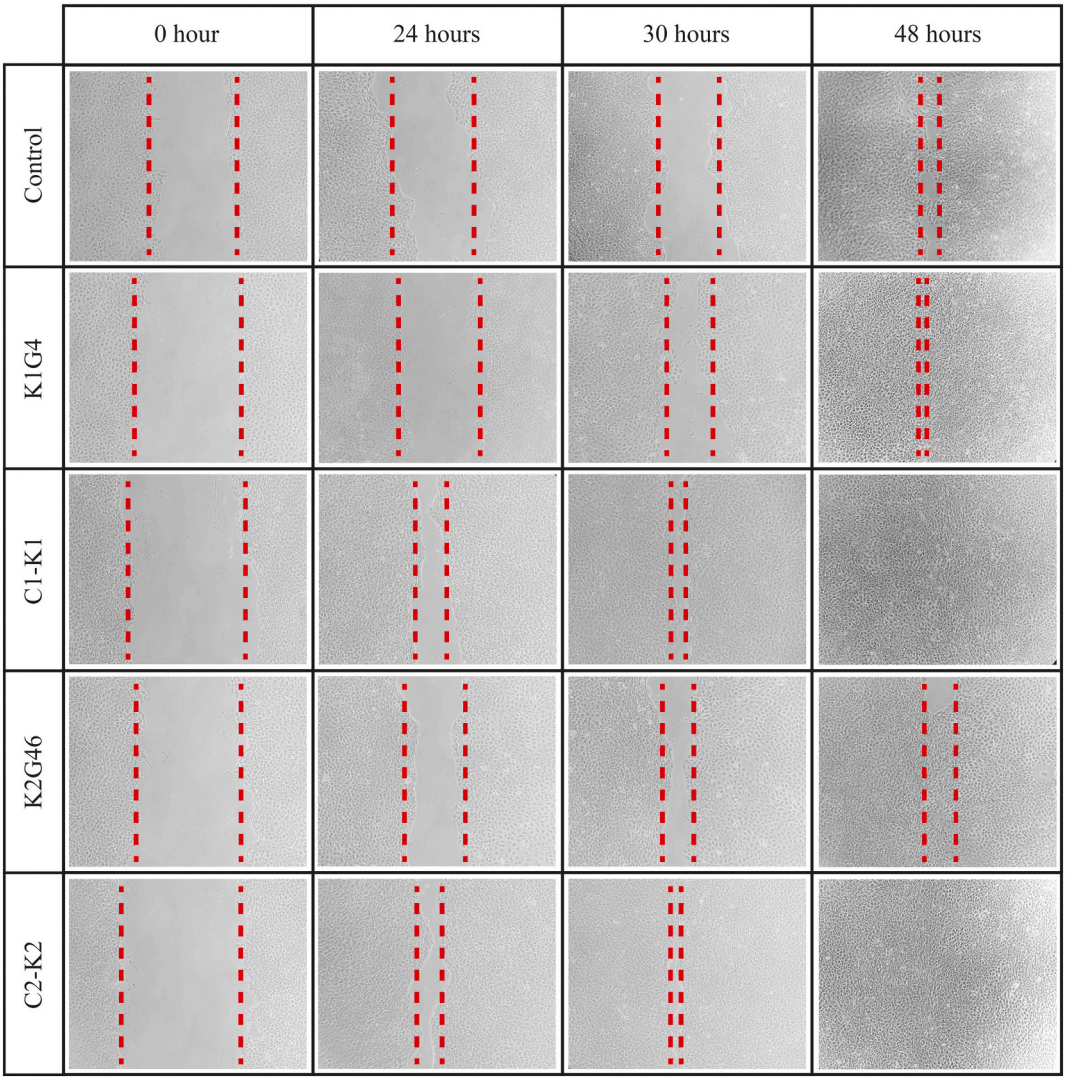

Fig. 9. Optical micrographs of the *in vitro* scratch assay with HaCaT cells. Micrographs were taken after 0, 24, 30 and 48 h of exposure to control, pure BNC (K1G4 and K2G46), and BNC-HA composites (C1-K1 and C2-K2). Images were captured at 100x magnification.

or *in-situ* modified BNC-HA composites in current and future medical applications. However, even the obtained outcomes are very promising, there are notable challenges to address. The co-culture system's scalability is still a major hurdle. Maintaining pH stability is essential, as larger volumes amplify pH fluctuations caused by increased metabolic activity. Ensuring uniform nutrient distribution and oxygenation is also crucial, as oxygen availability directly impacts BNC synthesis by *Komagataeibacter sp.* strains. Advanced aeration systems and optimized inoculum ratios for bacterial strains can prevent nutrient competition and support balanced growth.

Bioreactor design is pivotal, with airlift bioreactors offering controlled homogeneity, while modular setups can facilitate parallel production. Metabolic byproducts, such as gluconic and lactic acids, may inhibit microbial activity at larger scales, requiring solutions like periodic medium replacement or *in-situ* product removal. Efficient downstream processing methods are also necessary to maintain nanocomposite quality while ensuring scalability and cost-effectiveness. Finally, pilot-scale validation is indispensable to identify and address bottlenecks such as oxygen limitations, or unexpected microbial interactions. By addressing these challenges, the co-culture systems can transition smoothly to scaled up productions while maintaining high yields and product quality.

The limited number of studies exploring co-culture systems for the fabrication of materials for wound healing highlight the need for further investigations aiming to completely comprehend and optimize this approach. Additionally, even this study demonstrated the efficacy of the BNC-HA nanocomposites *in vitro*, *in vivo* testing will be necessary to determine the wound healing efficacy under real-application conditions. Addressing these challenges will be critical for advancing and scaling up the application of BNC-HA nanocomposites and realizing their full potential in clinical and industrial context.

CRediT authorship contribution statement

M. Brugnoli: Writing – review & editing, Writing – original draft, Methodology, Investigation. **J.P.F. Carvalho:** Writing – review & editing, Methodology, Investigation. **M.P. Arena:** Writing – review & editing. **H. Oliveira:** Writing – review & editing, Resources. **C. Vilela:** Writing – review & editing, Resources, Methodology. **C.S.R. Freire:** Writing – review & editing, Supervision, Resources, Methodology, Funding acquisition. **M. Gullo:** Writing – review & editing, Supervision, Resources, Funding acquisition, Conceptualization.

Funding

Part of this work was supported by the European Commission –

NextGenerationEU, Project SUS-MIRRI.IT "Strengthening the MIRRI Italian Research Infrastructure for Sustainable Bioscience and Bioeconomy", code n. IR0000005, and by the European Union – NextGenerationEUGrant, CN_00000033, Project "National Biodiversity Future Center – NBFC". CUP E93C22001090001. This work was also developed within the scope of the project CICECO-Aveiro Institute of Materials, UIDB/50011/2020 (DOI 10.54499/UIDB/50011/2020), UIDP/50011/2020 (DOI 10.54499/UIDP/50011/2020) & LA/P/0006/2020 (DOI 10.54499/LA/P/0006/2020), financed by national funds through the FCT/MEC (PIDDAC). FCT is acknowledged for the doctoral grants to J.P.F.C (2020.09018.BD, DOI 10.54499/2020.09018.BD) and the research contracts under Scientific Employment Stimulus to C.S.R.F. (DOI 10.54499/CEECIND/00464/2017/CP1459/CT0033), C.V. (DOI 10.54499/2021.01571.CEECIND/CP1659/CT0024) and H.O. (DOI 10.54499/CEECIND/04050/2017/CP1459/CT0023).

Declaration of competing interest

The authors declare that they have no known competing financial interests or personal relationships that could have appeared to influence the work reported in this paper.

Appendix A. Supplementary data

Supplementary data to this article can be found online at https://doi.org/10.1016/j.ijbiomac.2025.140208.

Data availability

All data was included in the manuscript in the form of figures. Sequences associated with this study have been deposited into the publicly repository Genbank under the accession number PQ518565.

References

[1] M. Gullo, S. La China, P.M. Falcone, P. Giudici, Biotechnological production of cellulose by acetic acid bacteria: current state and perspectives, Appl. Microbiol. Biotechnol. 102 (2018) 6885–6898, https://doi.org/10.1007/s00253-018-9164-5.
[2] S. Vid Potočnik, J. Trček Gorgieva, From nature to lab: sustainable bacterial cellulose production and modification with synthetic biology, Polymers 15 (2023) 3466, https://doi.org/10.3390/polym15163466.
[3] P. Cazón, G. Velázquez, M. Vázquez, Characterization of bacterial cellulose films combined with chitosan and polyvinyl alcohol: evaluation of mechanical and barrier properties, Carbohydr. Polym. 216 (2019) 72–85, https://doi.org/10.1016/j.carbpol.2019.03.093.
[4] S. Gea, E. Bilotti, C.T. Reynolds, N. Soykeabkeaw, T. Peijs, Bacterial cellulose–poly (vinyl alcohol) nanocomposites prepared by an in-situ process, Mater. Lett. 64 (2010) 901–904, https://doi.org/10.1016/j.matlet.2010.01.042.
[5] W.C. Lin, C.-C. Lien, H.-J. Yeh, C.-M. Yu, S.-h. Hsu, Bacterial cellulose and bacterial cellulose–chitosan membranes for wound dressing applications. Carbohydr. Polym. 94 (2013) 603–611. doi:https://doi.org/10.1016/j.carbpol.2013.01.076.
[6] A.R.P. Figueiredo, A.J.D. Silvestre, C.P. Neto, C.S.R. Freire, *In situ* synthesis of bacterial cellulose/polycaprolactone blends for hot pressing nanocomposite films production, Carbohydr. Polym. 132 (2015) 400–408, https://doi.org/10.1016/j.carbpol.2015.06.001.
[7] N.H.C.S. Silva, J.P. Mota, T.S. de Almeida, J.P.F. Carvalho, A.J.D. Silvestre, C. Vilela, C. Rosado, C.S.R. Freire, Topical drug delivery systems based on bacterial nanocellulose: accelerated stability testing, Int. J. Mol. Sci. 21 (2020) 1262, https://doi.org/10.3390/ijms21041262.
[8] D.F.S. Fonseca, J.P.F. Carvalho, V. Bastos, H. Oliveira, C. Moreirinha, A. Almeida, A.J.D. Silvestre, C. Vilela, C.S.R. Freire, Antibacterial multi-layered nanocellulose-based patches loaded with dexpanthenol for wound healing applications, Nanomaterials 10 (2020) 2469, https://doi.org/10.3390/nano10122469.
[9] L. Sabio, A. González, G.B. Ramírez-Rodríguez, J. Gutiérrez-Fernández, O. Bañuelo, M. Olivares, N. Gálvez, J.M. Delgado-López, J.M. Dominguez-Vera, Probiotic cellulose: antibiotic-free biomaterials with enhanced antibacterial activity, Acta Biomater. 124 (2021) 244–253, https://doi.org/10.1016/j.actbio.2021.01.039.
[10] L. Sabio, J.M. Dominguez-Vera, J. De Vicente, J.M. Delgado-López, Living cellulose materials with tunable viscoelasticity through probiotic proliferation, ACS Applied Bio Materials 6 (2022), https://doi.org/10.1021/acsabm.2c00814.
[11] G. Li, A.G. Nandgaonkar, Y. Habibi, W.E. Krause, Q. Wei, L.A. Lucia, An environmentally benign approach to achieving vectorial alignment and high microporosity in bacterial cellulose/chitosan scaffolds, RSC Adv. 7 (2017) 13678–13688, https://doi.org/10.1039/C6RA26049G.
[12] D.R. Ruka, G.P. Simon, K.M. Dean, *In situ* modifications to bacterial cellulose with the water insoluble polymer poly-3-hydroxybutyrate, Carbohydr. Polym. 92 (2013) 1717–1723, https://doi.org/10.1016/j.carbpol.2012.11.007.
[13] K. Jin, C. Jin, Y. Wu, Synthetic biology-powered microbial co-culture approach and application of bacterial cellulose-based composite materials, Carbohydr. Polym. 283 (2022) 119171, https://doi.org/10.1016/j.carbpol.2022.119171.
[14] R. Ding, S. Hu, M. Xu, Q. Hu, S. Jiang, K. Xu, P.-L. Tremblay, T. Zhang, The facile and controllable synthesis of a bacterial cellulose/polyhydroxybutyrate composite by co-culturing *Gluconacetobacter xylinus* and *Ralstonia eutropha*, Carbohydr. Polym. 252 (2021) 117137, https://doi.org/10.1016/j.carbpol.2020.117137.
[15] W. Qiao, Y. Qiao, G. Gao, Z. Liao, Z. Wu, P.E.J. Saris, H. Xu, M. Qiao, A novel co-cultivation strategy to generate low-crystallinity bacterial cellulose and increase nisin yields, Int. J. Biol. Macromol. 2022 (2020) 388–396, https://doi.org/10.1016/j.ijbiomac.2022.01.038.
[16] Y.-C. Huang, D. Khumsupan, S.-P. Lin, S.P. Santoso, H.-Y. Hsu, K.-C. Cheng, Production of bacterial cellulose (BC)/nisin composite with enhanced antibacterial and mechanical properties through co-cultivation of *Komagataeibacter xylinum* and *Lactococcus lactis* subsp. *lactis*, Int. J. Biol. Macromol. 258 (2024) 128977, https://doi.org/10.1016/j.ijbiomac.2023.128977.
[17] W. Qiao, C. Jia, J. Yang, G. Gao, D. Guo, X. Xu, Z. Wu, P.E.J. Saris, H. Xu, M. Qiao, Production of bacterial cellulose-based peptidopolysaccharide BC-L with anti-listerial properties using a co-cultivation strategy, Int. J. Biol. Macromol. 274 (2024) 133047, https://doi.org/10.1016/j.ijbiomac.2024.133047.
[18] E. Papakonstantinou, M. Roth, G. Karakiulakis, Hyaluronic acid: a key molecule in skin aging, Dermatoendocrinol 4 (2012) 253–258, https://doi.org/10.4161/derm.21923.
[19] S.A. de Oliveira, B.C. da Silva, I.C. Riegel-Vidotti, A. Urbano, P.C. de Sousa Faria-Tischer, C.A. Tischer, Production and characterization of bacterial cellulose membranes with hyaluronic acid from chicken comb, Int. J. Biol. Macromol. 97 (2017) 642–653, https://doi.org/10.1016/j.ijbiomac.2017.01.077.
[20] S. Tang, K. Chi, H. Xu, Q. Yong, J. Yang, J.M. Catchmark, A covalently cross-linked hyaluronic acid/bacterial cellulose composite hydrogel for potential biological applications, Carbohydr. Polym. 252 (2021) 117123, https://doi.org/10.1016/j.carbpol.2020.117123.
[21] K. Liu, J.M. Catchmark, Bacterial cellulose/hyaluronic acid nanocomposites production through co-culturing *Gluconacetobacter hansenii* and *Lactococcus lactis* under different initial pH values of fermentation media, Cellulose 27 (2020) 2529–2540, https://doi.org/10.1007/s10570-019-02924-w.
[22] K. Liu, J.M. Catchmark, Bacterial cellulose/hyaluronic acid nanocomposites production through co-culturing *Gluconacetobacter hansenii* and *Lactococcus lactis* in a two-vessel circulating system, Bioresour. Technol. 290 (2019) 121715, https://doi.org/10.1016/j.biortech.2019.121715.
[23] M. Brugnoli, I. Mazzini, S. La China, L. De Vero, M. Gullo, A microbial co-culturing system for producing cellulose-hyaluronic acid composite, Microorganisms 11 (2023) 1504, https://doi.org/10.3390/microorganisms11061504.
[24] S. La China, A. Bezzecchi, F. Moya, G. Petroni, S. Di Gregorio, M. Gullo, Genome sequencing and phylogenetic analysis of K1G4: a new *Komagataeibacter* strain producing bacterial cellulose from different carbon sources, Biotechnol. Lett. 42 (2020) 807–818, https://doi.org/10.1007/s10529-020-02811-6.
[25] S. Hestrin, M. Schramm, Synthesis of cellulose by *Acetobacter xylinum*. 2. Preparation of freeze-dried cells capable of polymerizing glucose to cellulose, Biochem. J. 58 (1954) 345–352, https://doi.org/10.1042/bj0580345.
[26] J.C. De Man, M. Rogosa, M.E. Sharpe, A medium for the cultivation of lactobacilli, J. Appl. Bacteriol. 23 (1960) 130–135, https://doi.org/10.1111/j.1365-2672.1960.tb00188.x.
[27] R.R. Navarro, K. Sumi, M. Matsumura, Improved metal affinity of chelating adsorbents through graft polymerization, Water Res. 33 (1999) 2037–2044, https://doi.org/10.1016/S0043-1354(98)00421-7.
[28] M. Gullo, C. Caggia, L. De Vero, P. Giudici, Characterization of acetic acid bacteria in "traditional balsamic vinegar", Int. J. Food Microbiol. 106 (2006) 209–212, https://doi.org/10.1016/j.ijfoodmicro.2005.06.024.
[29] M. Song, J.H. Im, J.H. Kang, D.J. Kang, A simple method for hyaluronic acid quantification in culture broth, Carbohydr. Polym. 78 (2009) 633–634, https://doi.org/10.1016/j.carbpol.2009.04.033.
[30] J.P.F. Carvalho, A.C.Q. Silva, V. Bastos, H. Oliveira, R.J.B. Pinto, A.J.D. Silvestre, C. Viliela, C.S.R. Freire, Nanocellulose-based patches loaded with hyaluronic acid and diclofenac towards aphthous stomatitis treatment, Nanomater 10 (2020) 628, https://doi.org/10.3390/nano10040628.
[31] L. Greenspan, Humidity fixed points of binary saturated aqueous solutions, J. Res. Natl. Bur. Stand. A Phys. Chem. 81 (1977) 89–96, https://doi.org/10.6028/jres.081A.011.
[32] T. Mosmann, Rapid colorimetric assay for cellular growth and survival: application to proliferation and cytotoxicity assays, J. Immunol. Methods 65 (1983) 55–63, https://doi.org/10.1016/0022-1759(83)90303-4.
[33] N.C.S. Silva, P. Garrido-Pascual, C. Moreirinha, A. Almeida, T. Palomares, A. Alonso-Varona, C. Vilela, C.S.R. Freire, Multifunctional nanofibrous patches composed of nanocellulose and lysozyme nanofibers for cutaneous wound healing, Int. J. Biol. Macromol. 165 (2020) 1198–1210, https://doi.org/10.1016/j.ijbiomac.2020.09.249.
[34] R Core Team, R: A Language and Environment for Statistical Computing, R Foundation for Statistical Computing, Vienna, Austria, 2022. https://www.R-project.org/.
[35] D. Mamlouk, Insight into Physiology and Functionality of Acetic Acid bacteria Through a Multiphasic Approach, Ph.D. Thesis Dissertation,, University of Modena and Reggio Emilia, Reggio Emilia, Italy, 2012.

[36] P.R. Chawla, I.B. Bajaj, S.A. Survase, R.S. Singhal, Microbial cellulose: fermentative production and applications, Food Sci. Biotechnol. 47 (2009) 107–124.
[37] S.M.A.S. Keshk, Bacterial cellulose production and its industrial applications, Int. J. Bioprocess Biotech. 4 (2014) 1, https://doi.org/10.4172/2155-9821.1000150.
[38] M. Brugnoli, F. Robotti, S. La China, K. Anguluri, H. Haghighi, S. Bottan, A. Ferrari, M. Gullo, Assessing effectiveness of *Komagataeibacter* strains for producing surface-microstructured cellulose via guided assembly-based biolithography, Sci. Rep. 11 (2021) 19311, https://doi.org/10.1038/s41598-021-98705-2.
[39] S. La China, G. Zanichelli, L. De Vero, M. Gullo, Oxidative fermentations and exopolysaccharides production by acetic acid bacteria: a mini review, Biotechnol. Lett. 40 (2018) 1289–1302, https://doi.org/10.1007/s10529-018-2591-7.
[40] W. Li, X. Huang, H. Liu, H. Lian, B. Xu, W. Zhang, X. Sun, W. Wang, S. Jia, C. Zhong, Improvement in bacterial cellulose production by co-culturing *Bacillus cereus* and *Komagataeibacter xylinus*, Carbohydr. Polym. 313 (2023) 120892, https://doi.org/10.1016/j.carbpol.2023.120892.
[41] A.J. Akki, L.D. Hiremath, R.R. Badkillaya, Harnessing symbiotic association of lactic acid bacteria and cellulose-synthesizing bacteria for enhanced biological activity, Iran. J. Sci. 48 (2024) 311–320, https://doi.org/10.1007/s40995-023-01567-8.
[42] F. Lasagni, S. Cassanelli, M. Gullo, How carbon sources drive cellulose synthesis in two *Komagataeibacter xylinus* strains, Sci. Rep. 14 (2024) 20494, https://doi.org/10.1038/s41598-024-71648-0.
[43] J.H. Sze, J.C. Brownlie, C.A. Love, Biotechnological production of hyaluronic acid: a mini review, 3 Biotech 6 (2016) 67, https://doi.org/10.1007/s13205-016-0379-9.
[44] K. Anguluri, S. La China, M. Brugnoli, S. Cassanelli, M. Gullo, Better under stress: improving bacterial cellulose production by *Komagataeibacter xylinus* K2G30 (UMCC 2756) using adaptive laboratory evolution, Front. Microbiol. 13 (2022) 994097, https://doi.org/10.3389/fmicb.2022.994097.
[45] Y. Wang, J. Wu, M. Lv, Z. Shao, M. Hungwe, J. Wang, X. Bai, J. Xie, Y. Wang, W. Geng, Metabolism characteristics of lactic acid bacteria and the expanding applications in food industry, Front. Bioeng. Biotechnol. 9 (2021), https://doi.org/10.3389/fbioe.2021.612285.
[46] A. Maleki, A.-L. Kjøniksen, B. Nyström, Effect of pH on the behavior of hyaluronic acid in dilute and semidilute aqueous solutions, Macromol. Symp. 274 (2008) 131–140, https://doi.org/10.1002/masy.200851418.
[47] M. Faria, C. Vilela, F. Mohammadkazemi, A.J.D. Silvestre, C.S.R. Freire, N. Cordeiro, Poly(glycidyl methacrylate)/bacterial cellulose nanocomposites: preparation, characterization and post-modification, Int. J. Biol. Macromol. 127 (2019) 618–627, https://doi.org/10.1016/j.ijbiomac.2019.01.133.
[48] T.D. Lopes, I.C. Riegel-Vidotti, A. Greinb, C.A. Tischer, P.C. de Sousa Faria-Tischer, Bacterial cellulose and hyaluronic acid hybrid membranes: production and characterization, Int. J. Biol. Macromol. 67 (2014) 401–408, https://doi.org/10.1016/j.ijbiomac.2014.03.047.
[49] S. Barbi, C. Taurino, S. La China, K. Anguluri, M. Gullo, M. Montorsi, Mechanical and structural properties of environmental green composites based on functionalized bacterial cellulose, Cellulose 28 (2021) 1431–1442, https://doi.org/10.1007/s10570-020-03602-y.
[50] T. Mirzayeva, J. Čopíková, F. Kvasnička, R. Bleha, A. Synytsya, Screening of the chemical composition and identification of hyaluronic acid in food supplements by fractionation and Fourier-transform infrared spectroscopy, Polymers 13 (2021) 4002, https://doi.org/10.3390/polym13224002.
[51] P.C.S. Faria-Tischer, C.A. Tischer, L. Heux, S. Le Denmat, C. Picart, M.-R. Sierakowski, J.-L. Putaux, Preparation of cellulose II and IIII films by allomorphic conversion of bacterial cellulose I pellicles, Mater. Sci. Eng. C 51 (2015) 167–173, https://doi.org/10.1016/j.msec.2015.02.025.
[52] S. Gorgieva, U. Jančič, E. Cepec, J. Trček, Production efficiency and properties of bacterial cellulose membranes in a novel grape pomace hydrolysate by *Komagataeibacter melomenusus* AV436^T and *Komagataeibacter xylinus* LMG 1518, Int. J. Biol. Macromol. 244 (2023) 125368, https://doi.org/10.1016/j.ijbiomac.2023.125368.
[53] M. Zeng, A. Laromaine, A. Roig, Bacterial cellulose films: influence of bacterial strain and drying route on film properties, Cellulose 21 (2014) 4455–4469, https://doi.org/10.1007/s10570-014-0408-y.
[54] J.C. Bi, S.-X. Liu, C.-F. Li, J. Li, L.-X. Liu, J. Deng, Y.-C. Yang, Morphology and structure characterization of bacterial celluloses produced by different strains in agitated culture, J. Appl. Microbiol. 117 (2014) 1305–1311, https://doi.org/10.1111/jam.12619.
[55] P. Singhsa, R. Narain, H. Manuspiya, Physical structure variations of bacterial cellulose produced by different *Komagataeibacter xylinus* strains and carbon sources in static and agitated conditions, Cellulose 25 (2018) 1571–1581, https://doi.org/10.1007/s10570-018-1699-1.
[56] G. Li, L. Wang, Y. Deng, Q. Wei, Research progress of the biosynthetic strains and pathways of bacterial cellulose, J. Ind. Microbiol. Biotechnol. 49 (2022), https://doi.org/10.1093/jimb/kuab071.
[57] H. Jiang, Z. Song, Y. Hao, X. Hu, X. Lin, S. Liu, C. Li, Effect of co-culture of *Komagataeibacter nataicola* and selected *lactobacillus fermentum* on the production and characterization of bacterial cellulose, LWT 173 (2023) 114224, https://doi.org/10.1016/j.lwt.2022.114224.
[58] K. Chi, J.M. Catchmark, The influences of added polysaccharides on the properties of bacterial crystalline nanocellulose, Nanoscale 39 (2017) 15144, https://doi.org/10.1039/C7NR05615J.
[59] C. Vilela, H. Oliveira, A. Almeida, A.J.D. Silvestre, C.S.R. Freire, Nanocellulose-based antifungal nanocomposites against the polymorphic fungus *Candida albicans*, Carbohydr. Polym. 217 (2019) 207–216, https://doi.org/10.1016/j.carbpol.2019.04.046.
[60] R. Naomi, R.B.H. Idrus, M.B. Fauzi, Plant- vs. bacterial-derived cellulose for wound healing: a review, Int. J. Environ. Res. Public Health 17 (2020) 6803, https://doi.org/10.3390/ijerph17186803.
[61] Y. Jia, W. Zhu, M. Zheng, M. Huo, C. Zhong, Bacterial cellulose/hyaluronic acid composite hydrogels with improved viscoelastic properties and good thermodynamic stability, Plast. Rubber Compos. 47 (2018) 165–175, https://doi.org/10.1080/14658011.2018.1447340.
[62] Y. Li, S. Qing, J. Zhou, G. Yang, Evaluation of bacterial cellulose/hyaluronan nanocomposite biomaterials, Carbohydr. Polym. 103 (2014) 496–501, https://doi.org/10.1016/j.carbpol.2013.12.059.
[63] A. Kalra, A. Lowe, A.M. Al-Jumaily, Mechanical behaviour of skin: a review, J. Mater. Sci. Eng. 5. doi:https://doi.org/10.4172/2169-0022.1000254.
[64] S.J.M. Yazdi, J. Baqersad, Mechanical modeling and characterization of human skin: a review, J. Biomech. 130 (2022) 110864, https://doi.org/10.1016/j.jbiomech.2021.110864.
[65] M.F. Griffin, B.C. Leung, Y. Premakumar, M. Szarko, P.E. Butler, Comparison of the mechanical properties of different skin sites for auricular and nasal reconstruction, Otolaryngol. Head Neck Surg. 46 (2017) 1–9, https://doi.org/10.1186/s40463-017-0210-6.
[66] W.S. Chang, H.H. Chen, Physical properties of bacterial cellulose composites for wound dressings, Food Hydrocoll. 53 (2016) 75–83, https://doi.org/10.1016/j.foodhyd.2014.12.009.
[67] A. Al-Maharma, N. Al-Huniti, Critical review of the parameters affecting the effectiveness of moisture absorption treatments used for natural composites, J. Compos. Sci. 3 (2019) 27, https://doi.org/10.3390/jcs3010027.
[68] S. Adepu, M. Khandelwal, *Ex-situ* modification of bacterial cellulose for immediate and sustained drug release with insights into release mechanism, Carbohydr. Polym. 249 (2020) 116816, https://doi.org/10.1016/j.carbpol.2020.116816.
[69] M. Ul-Islam, T. Khan, J.K. Park, Water holding and release properties of bacterial cellulose obtained by *in situ* and *ex situ* modification, Carbohydr. Polym. 88 (2012) 596–603, https://doi.org/10.1016/j.carbpol.2012.01.006.
[70] R. Ghosh, P. Singh, A.H. Pandit, U. Tariq, B.K. Bhunia, A. Kumar, Emerging technological advancement for chronic wound treatment and their role in accelerating wound healing, ACS Appl. Bio Mater. 7 (2024), https://doi.org/10.1021/acsabm.4c01064.
[71] ISO 10993-5:2009(E), Biological Evaluation of Medical Composites - Part 5: Tests for in Vitro Cytotoxicity, 2009.
[72] Y.M. Chen, T. Xi, C. Gao, In vitro cytotoxicity of bacterial cellulose scaffolds used for tissue-engineered bone, J. Bioact. Compat. Polym. 24 (2009) 137–145, https://doi.org/10.1177/0883911509102710.
[73] M. Sharma, K. Sahu, S.P. Singh, B. Jain, Wound healing activity of curcumin conjugated to hyaluronic acid: *in vitro* and *in vivo* evaluation, Artif. Cells Nanomed. Biotechnol. 46 (2018) 1009–1017, https://doi.org/10.1080/21691401.2017.1358731.
[74] X. Wang, J. Tang, J. Huang, M. Hui, Production and characterization of bacterial cellulose membranes with hyaluronic acid and silk sericin, Colloids Surf. B: Biointerfaces 195 (2020) 111273, https://doi.org/10.1016/j.colsurfb.2020.111273.
[75] Y. Kawano, V. Patrulea, E. Sublet, G. Borchard, T. Iyoda, R. Kageyama, A. Morita, S. Seino, H. Yoshida, O. Jordan, T. Hanawa, Wound healing promotion by hyaluronic acid: effect of molecular weight on gene expression and in vivo wound closure, Pharmaceuticals 14 (2021) 301, https://doi.org/10.3390/ph14040301.
[76] A.C.Q. Silva, M. Mendes, C. Vitorino, U. Montejo, A. Alonso-Varona, A.J. D. Silvestre, C. Vilela, C.S.R. Freire, Trilayered nanocellulose-based patches loaded with acyclovir and hyaluronic acid for the treatment of herpetic lesions, Int. J. Biol. Macromol. 277 (2024) 133843, https://doi.org/10.1016/j.ijbiomac.2024.133843.